UNIVERSIDAD DE CHILE
FACULTAD DE CIENCIAS FÍSICAS Y MATEMÁTICAS
DEPARTAMENTO DE FÍSICA

# ASPECTS OF ANTIFERROMAGNETIC SPINTRONICS

TESIS PARA OPTAR AL GRADO DE MAGÍSTER EN CIENCIAS, MENCIÓN FÍSICA

CAMILO EDGARDO ULLOA OSORIO

PROFESOR GUÍA:
ÁLVARO NÚÑEZ VÁSQUEZ

MIEMBROS DE LA COMISIÓN:
RODRIGO ARIAS FEDERICI
LUIS FOÀ TORRES
PEDRO LANDEROS SILVA

Este trabajo ha sido parcialmente financiado por Proyecto Fondecyt No. 1150072, Proyecto Basal No. FB0807- CEDENNA, y Anillo de Ciencia y Tecnología No. ACT 1117

SANTIAGO DE CHILE
2016

RESUMEN DE LA MEMORIA PARA OPTAR
AL TÍTULO DE MAGÍSTER EN CIENCIAS, MENCIÓN FÍSICA
POR: CAMILO EDGARDO ULLOA OSORIO
FECHA: 2016
PROF. GUÍA: SR. ÁLVARO NÚÑEZ VÁSQUEZ

# ASPECTS OF ANTIFERROMAGNETIC SPINTRONICS

La spintrónica se perfila como una de las corrientes mas atractivas y prometedoras dentro de la materia condensada gracias a la diversidad de fenómenos presentes, como el efecto Hall de spin, la magneto-resistencia gigante. En la spintrónica el estudio de materiales antiferromagnéticos es interesante pues dentro de sus propiedades se encuentran su abundancia natural y la posibilidad de disminuir las escalas temporal y espacial de los fenómenos presentes en ellos. Un ejemplo es la utilización de estos materiales en memorias magnéticas, pues gracias a la ausencia de magnetización neta en un material antiferromagnético es posible almacenar información en regiones de menor tamaño debido a la nula interacción dipolar entre dominios magnéticos. Esta tesis está compuesta de tres trabajos teóricos orientados al desarrollo de la spintrónica antiferromagnética.

En la primera parte se presenta la teoría efectiva de un sistema antiferromagnético no colineal. Para esto consideramos un sistema anisotrópico y con interacción de intercambio entre spines vecinos. A través de un parámetro de orden perteneciente al grupo de rotaciones estudiamos la dinámica de las excitaciones de baja energía del sistema obteniendo como resultado una familia de solitones topológicos que están descritos por la ecuación de sine-Gordon. Finalmente comparamos nuestros resultados con simulaciones numéricas de un sistema de momentos magnéticos obteniendo resultados completamente concordantes.

La segunda parte corresponde al estudio de un cristal magnónico antiferromagnético. A partir de una teoría fenomenológica estudiamos la dinámica del campo de magnetización bajo el efecto de interacción de intercambio, y anisotropía uniaxial. A través de una modulación periódica de la anisotropía y del campo magnético caracterizamos el espectro de ondas de spín y las estructura de bandas del sistema.

En la tercera y última parte se presenta el estudio de la generación de corrientes de spin mediante deformaciones de una red antiferromagnética gracias a efectos cuánticos. Este fenómeno, conocido como efecto piezospintrónico, es estudiado en dos modelos de interés: grafeno antiferromagnético y zinc-blende antiferromagnético. Este efecto, en conjunto con el efecto Hall de spín inverso pueden ser útiles para la detección de corrientes de spín puras.

RESUMEN DE LA MEMORIA PARA OPTAR
AL TÍTULO DE MAGÍSTER EN CIENCIAS, MENCIÓN FÍSICA
POR: CAMILO EDGARDO ULLOA OSORIO
FECHA: 2016
PROF. GUÍA: SR. ÁLVARO NÚÑEZ VÁSQUEZ

# ASPECTS OF ANTIFERROMAGNETIC SPINTRONICS

Spintronics is one of the most attractive and promising areas in condensed matter due to the diversity of phenomena present in it as the spin Hall effect and the giant magnetoresistance. In spintronics the study of antiferromagnetic materials is interesting due to their natural abundance and the possibility of decreasing the temporal and spatial scale of the phenomena in which they are involved. One example of this is the use of antiferromagnetic materials in magnetic memories, where due to the absence of net magnetization it is possible to store information in smaller regions because of the null dipolar interaction between domains. This thesis is made of three theoretical works focused in different aspects of antiferromagnetic spintronics.

In the first chapter we present the effective theory of a non collinear antiferromagnet. For this we consider an anisotropic system with exchange interaction among neighbor spins. By making use of an order parameter in the rotation group we study the dynamics of low energy excitations of the system obtaining as result a family of topological solitons which are described by the sine-Gordon equation. Finally we compare our results with numerical simulations of a system of magnetic moments obtaining totally concordant results.

The second chapter corresponds to the study of an antiferromagnetic magnonic crystal. From a phenomenological theory we study the dynamics of the magnetization field under the effect of exchange interaction and uniaxial anisotropy. Through a periodic modulation of the anisotropy and of the magnetic field we characterize the spin wave spectra and the band structure of the system.

In the third and last chapter we show the study of generation of spin currents by deformation of an antiferromagnetic lattice thanks to quantum mechanical effects. This phenomenon, known as piezospintronic effect, is studied in two interesting models: antiferromagnetic graphene and antiferromagnetic zinc-blende. This effect together with the inverse spin Hall effect could be useful for the detection of pure spin currents.

*None of them along the line know what any of it is worth.* Bob Dylan.

# Agradecimientos

Quiero agradecer a todos quienes me han apoyado a lo largo de este camino. Amigos, familia, compañeros, a quienes no nombraré porque una lista tan larga no alcanza en estas páginas. Por supuesto debo agradecer a mi profesor guía Álvaro por el apoyo en todo ámbito.

Gracias totales.

# Contents

# List of Figures

# Chapter 1

# Introduction

Spintronics is the area of condensed matter physics that studies the properties of the electron spin with the aim of improving the efficiency of electronic devices and to enrich them with new functionalities and phenomena that interlink the spin and charge degrees of freedom [1, 2, 3, 4]. Current spintronics applications are centered around magnetic storage of information and sensing devices based on key advances in the field, such as tunneling magnetoresistance (TMR), giant magneto resistance (GMR) and electrical spin injection. Nevertheless the proper control of spin and magnetism in a wide family of materials and their nanostructures has the potential for a much broader impact.

In particular, in this work we are involved into antiferromagnetic spintronics. Antiferromagnetic materials are internally magnetic, but the internal order of the microscopic magnetic moments cancels the macroscopic magnetization. This makes magnetism in antiferromagnetic materials invisible to their external environment. Because of this Louis Néel, Nobel prize in Physics in 1970 for *fundamental work and discoveries concerning antiferromagnetism and ferrimagnetism which have led to important applications in solid state physics*, said that antiferromagnetic materials are *extremely interesting from the theoretical viewpoint, but do not seem to have any applications*[5]. Since then, a lot of people have been working in order to show that Néel was wrong. Some examples of these works are shown in the recent review by Jungwirth et al [6].

Along this chapter we introduce some elementary concepts which are relevant to understand the rest of the text.

## 1.1 The spin and the electron

Electrons were discovered by J. J. Thompson in 1897, but they hid a fascinating property until G. Uhlenbeck and S. Gouldsmit proposed the *spin* [7] to explain some properties of the atomic spectra. Later W. Pauli and P. A. M. Dirac developed the relativistic quantum theory of electrons in which the spin, as an intrinsic property, arises naturally[8, 9]. A wrong but useful cartoon of the spin is the idea that electrons 'spins' around one axis, just as the earth rotates around herself. Of course this cartoon is wrong because electrons are point-like particles so they can not rotate around themselves, but electrons still have intrinsic angular momentum. In classical electrodynamics, a solid sphere rotating with charge $q$ generates an magnetic dipole $\mu$ proportional to the angular momentum of the sphere. In the quantum mechanical picture, the electron will generate a magnetic moment proportional to its spin

$$\mu = -\gamma \mathbf{S}, \tag{1.1}$$

where $\gamma = g\mu_B/\hbar$ is known as the gyromagnetic ratio, $g$ is the Landé factor, $\mu_B$ is the Bohr magneton, and $\hbar$ is Planck constant. The spin of a free electron is a quantity which has a magnitude $|\mathbf{S}| = \hbar/2$ and, as it is a vector quantity, has three components.

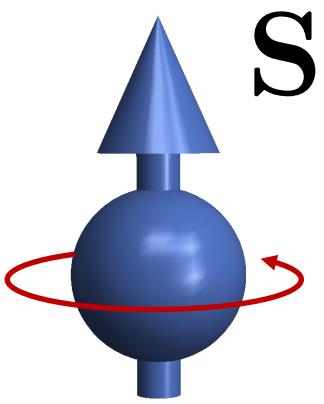


Figure 1.1: Classical cartoon of the intrinsic angular momentum **S** of an electron. Because of this intrinsic momenta an electron can be seen as a magnetic moment.

## 1.2 Magnetic ordering

Materials are made out of elements (atoms), which in their ground state have a finite number of electrons depending on the number of protons they have in the nucleus. Electrons arrange themselves in the allowed orbitals around the nucleus following Pauli exclusion principle and Hund rules so they are often arranged in pairs spin up - spin down which cancel the magnetic effect of the spins. Nevertheless there are some materials in which electrons are arranged in such way that some of the electrons might be unpaired at the valence orbital, then the total spin of these materials is non zero (typically transition metals, third to tenth column of periodic table). These materials are called magnetic materials.

There are several types of magnetic materials. In paramagnetic materials the electronic spins align parallel to an external magnetic field and this enhances the magnetic field inside the material. In diamagnetic materials the effect is exactly the opposite, the spins align anti-parallel to the field and that diminishes the magnetic field inside the material. These two families of magnetic materials share a particular property. Just as the external magnetic field disappears the alignment of the spins is lost, so there is not a permanent effect. On the other hand, ferromagnets and antiferromagnets have a strong magnetic ordering due to their high exchange interaction.

Exchange interaction is a quantum mechanical effect such that spins align relatively parallel or antiparallel. This fact was pointed out independently by W. Heisenberg and P.A.M Dirac in 1926 [10, 11]. The usual way to express this interaction is

$$E_{ex} = J\mathbf{S}_1 \cdot \mathbf{S}_2. \tag{1.2}$$

Equation (1.2) explains why (anti)ferromagnetic materials exist and their order is robust.

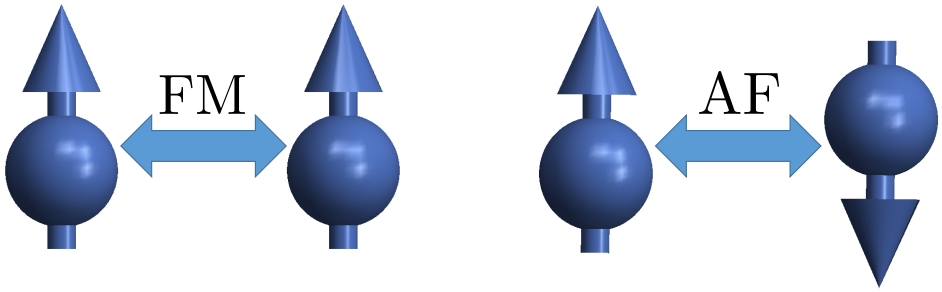


Figure 1.2: Cartoons of consequences of exchange interaction between two spins. If the exchange constant $J < 0$, the energy is a minimum when spins align parallel. This is known as ferromagnetic configuration. If the exchange constant $J > 0$, the minimum energy is find when spins are anti-parallel. This is known as antiferromagnetic configuration.

The magnetic ordering of materials is lost when they are heated up over a certain temperature. For ferromagnetic materials this critical temperature is known as Curie's temperature $T_C$ while for antiferromagnets is known as Néel temperature $T_N$. In general most of materials become paramagnetic above the mentioned temperatures. Below $T_C$ ferromagnets

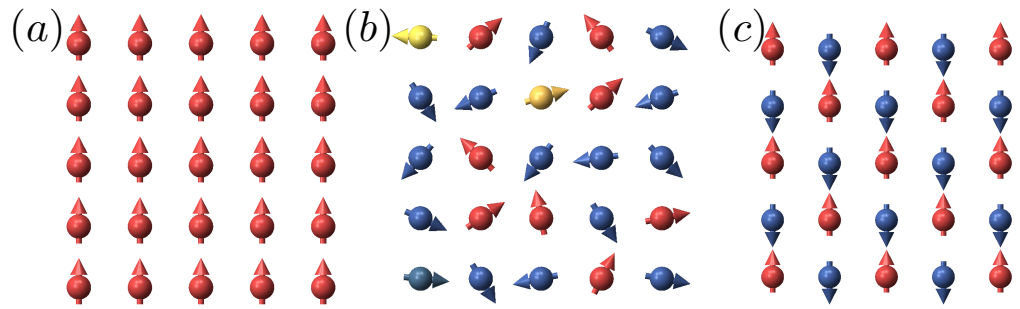


Figure 1.3: Cartoons of different kinds of magnetic order. (a) Ferromagnetic. (b) Paramagnetic. (c) Antiferromagnetic.

exhibit macroscopic magnetization and this property has been widely used along the human history, from compasses to hard drives. On the other hand antiferromagnets do not exhibit magnetization due to their particular magnetic order which cancels local magnetic moments, making them invisible to external magnetic fields. Because of this they seemed to be useless for practical purposes, but today many of us think that this remarkable property can be turned into an advantage against ferromagnetic materials. Due to the absence of magnetization the dipolar interaction between domains is totally negligible. This opens the possibility of diminishing the spatial scale of the phenomena present in these materials.

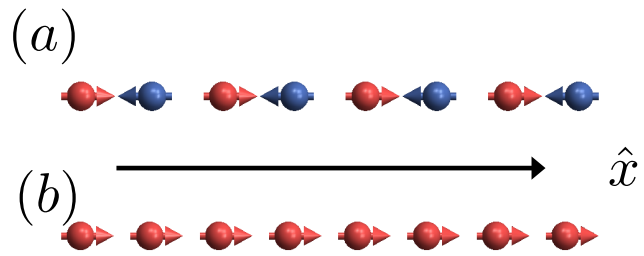


Figure 1.4: Cartoon of two different magnetic phase of a chain of spins under the influence of anisotropy along the $\hat{x}$ axis. (a) Antiferromagnetic chain. (b) Ferromagnetic chain.

Another important discovery made by L. Néel was that the anisotropy effects have the same consequences in ferromagnetic and antiferromagnetic materials. For example, lets consider a chain of magnetic moments as in Fig 1.2. Néel figured out that independently of the ferro/antiferromagnetic ordering, the energy associated with the anisotropy of the system to lie along a certain axis $\hat{x}$ has the form

$$E_{\text{ani}} = -K(\mathbf{S} \cdot \hat{x})^2. \tag{1.3}$$

This means that spins prefer to be aligned along $\hat{x}$ direction if $K > 0$. This effect adds remarkable properties to magnetic systems, as we show along this thesis. Of course depending on the sign of the value $K$ the effect on the system can be the opposite. If $K < 0$ the $\hat{x}$ axis is not likely for the spins, in this case we call it hard axis anisotropy and the spins lie in a plane perpendicular to $\hat{x}$ (also called easy plane).

## 1.3 Antiferromagnetic order

The antiferromagnetic order is described through different roads. In particular in some chapters of this thesis we focus in the long wavelength description of this order. Due to the nature of the antiferromagnetic order is not possible to perform a direct gradient expansion of the magnetization because it is not a soft function. Then is not trivial to obtain the continuum approximation of an antiferromagnetic system directly in terms of the magnetization. One way to perform this expansion was introduced by Haldane in 1983 [12] for a bipartite lattice as follows,

$$\mathbf{S}_{\text{i}} = \eta_{\text{i}} \mathbf{n}(\mathbf{x}_{\text{i}}) \sqrt{1 - \left| \frac{\mathbf{m}(\mathbf{x}_{\text{i}})}{S} \right|^2} + \frac{\mathbf{m}(\mathbf{x}_{\text{i}})}{S}, \tag{1.4}$$

where $\eta_{\rm i} = {\rm e}^{{\rm i}\mathbf{X}_{\rm i}\vec{\pi}} = (-1)^{\rm i}$ has opposite sign on the two sublattices. The field $\mathbf{n}$ is the unimodular *Neel field* (also known as *staggered magnetization*),

$$|\mathbf{n}(\mathbf{x}_{\rm i})| = 1. \tag{1.5}$$

$\mathbf{m}$ is the transverse *canting field* (also known as *magnetization field*), which is chosen to obey

$$\mathbf{n}(\mathbf{x}_{\rm i}) \cdot \mathbf{m}(\mathbf{x}_{\rm i}) = 0. \tag{1.6}$$

In equilibrium $\mathbf{m}(x) = 0$ and $\mathbf{n}(x) \neq 0$. Now the antiferromagnetic order can be described by two fields whose are soft along the space and now is possible to perform a gradient expansion of these fields to obtain the long wavelength limit of the system.

## 1.4 Outline

With the previous sections the reader is in conditions to walk through this thesis with the basic concepts in his pocket. This will lead the reader at least to understand the phenomenology of the physics involved in the three works which are the main body of this text.

In the second chapter we develop a theory of a non collinear antiferromagnet based in a model for $Mn_3Ir$. We characterize the low energy excitations of the magnetic system by performing a gradient expansion of the order parameter which belongs to $SO(3)$ (rotation group). We find a family of topological solitons and we discuss their properties. This work was published in Physical Review B on April 29th, 2016.

The third chapter consists of making use of the continuum theory of an antiferromagnetic system to characterize the magnonic bands of a system which has an periodic anisotropy or is under a periodic external magnetic field. This leads to an antiferromagnetic magnonic crystal which can be engineered by modifying either the periodicity and the magnitude of the anisotropy/magnetic field change. This work was published in Physical Review B on December 17th, 2015.

In the fourth chapter we study the generation of pure spin currents by deformations of a lattice. We analyze two models of interest: antiferromagnetic graphene, and antiferromagnetic zinc-blende. This effect is known as piezospintronic effect and could lead, in cooperation with other known spintronic effects, to a robust generation (or detection) of pure spin currents.

In the several appendices we show some explicit calculations and advanced topics related with the contents of this thesis. In Appendix A we show the path integral formulation of a spin system. This is a natural way to introduce the the Berry phase in spin systems. Appendix B introduces the Landau-Lifshitz-Gilbert equation. We also show two numerical methods to solve this equation for a spin system. In Appendix C we show the explicit calculation of the effective action of a non collinear antiferromagnet. Also we show explicit calculations which lead to the spin wave spectra for two known solutions. In Appendix D we analyze some solutions of the sine-Gordon equation by two different roads, by performing a direct integration of the equation, and making use of Bäcklund transformations. This leads to the solutions utilized in Chapter 2. In the last appendix we show the explicit calculation that leads to the spin wave spectra of Chapter 3.

# Chapter 2

# Soliton-like textures in non collinear antiferromagnets

In this chapter we show that proper control of magnetization textures can be achieved in non-collinear antiferromagnets. This opens up the versatile toolbox of domain wall manipulation in the context of a new family of materials. In this way, we show that non-collinear antiferromagnets are a good prospect for applications in the context of antiferromagnetic spintronics. As in many non-collinear antiferromagnets the order parameter field takes values in SO(3). By performing a gradient expansion in the energy functional we derive an effective theory that accounts for the physics of the magnetization of long wavelength excitations. We apply our formalism to static and dynamic textures such as domain walls and localized oscillations, and identify topologically protected textures that are spatially localized. Our results are applicable to the exchange-bias materials $Mn_3X$, with $X = Ir,\ Rh,\ Pt$.

## 2.1 Introduction

In antiferromagnetic materials the exchange coupling among neighboring spins favor antiparallel arrangements as we have explained in Sec. 1.2. Because of this interaction the system is led to an ordered magnetic state where the magnetization of different sublattices is oriented in a way that the overall magnetization is cancelled. This order drives the system into a robust collective behavior with soft modes that can be controlled with the aid of external magnetic fields. Recently, the notion that spintronic effects analogous to the ones in ferromagnets can be exhibited by antiferromagnetic systems has received attention from the theoretical [1, 2, 13, 14, 15, 16, 17] and experimental[18, 19, 20, 21, 22, 23] viewpoints. The advantages of antiferromagnetic systems come from a variety of reasons. For example they do not display stray fields, they display high frequency response (in the terahertz range), and finally the fact that antiferromagnetism is observed more often and at much softer conditions than ferromagnetism.

A promising development in the context of antiferromagnetic spintronics is the fact that

it is possible to engineer magnetic textures, such as domain walls (DW), in antiferromagnetic systems [24]. The problem of domain wall manipulation in antiferromagnetic systems has been studied in some recent papers[25, 26, 27, 28, 29, 30] where, using the collective coordinates approach, it was shown that the domain wall center obeys a Newton's law of motion. This opens the possibility of implementing domain wall control over antiferromagnets in the same fashion as it is done in ferromagnets. In ferromagnetic systems, magnetization textures, smooth modulations in the magnetization field, can be controlled in a diversity of manners, for example through the action of external fields or currents. Research in the field of magnetic domain wall manipulation has been growing steadily[31]. The driving force behind this research is the potential applications in the context of information technologies. An example of these applications, is the racetrack[32] configuration where domain walls are driven across a ferromagnetic wire by a current. Domain wall manipulation has also been shown as an alternative to electronic logic circuits[33].

In this work we propose that magnetic textures can also be found and controlled in non-collinear antiferromagnets. That is antiferromagnets whose underlying magnetic sub-lattices are not oriented along the same magnetic axis. Our main result is the theoretical characterization of the dynamics of domain walls in a non-collinear antiferromagnet. While our qualitative results apply to a wide family of non-collinear antiferromagnets, we will focus our attention to the magnetic degrees of freedom $Mn_3Ir$. This material has been studied extensively due to its importance as the pinning agent in exchange bias controlled spin-valves devices. $Mn_3Ir$ is regarded as a crystal with fcc structure with Mn atoms lying of the centers of the faces of each cube. The $Mn$ sublattices are two-dimensional kagome lattices lying in the planes perpendicular to the (111) direction. Due to the frustration within each triangular plaquette, isolated isotropic kagome lattices are known examples of disordered spin systems [34, 35, 36, 37]. On the contrary the $Mn$ spins in $Mn_3Ir$ display a quite strong three-sublattice triangular (T1) magnetic order up to a transition temperature of $\sim 950\ K$[38, 39]. The stability of magnetic order is due primarily to the exchange interaction among the kagome planes and to anisotropy [40, 41, 42]. Following [43], we use as a minimal model for the physics of the magnetization in $Mn_3Ir$ we start with a single nearest neighbour antiferromagnetically coupled kagome lattice of classical spins with appropriately tuned anisotropy terms.

## 2.2 Basic Model

The minimal model for magnetization dynamics of the Mn atoms in a (111) plane of $Mn_3Ir$ starts from a system of classical spins located at the vertices of a kagome lattice. These spins correspond to the magnetic degrees of freedom of the planes perpendicular to the (111) direction. The Hamiltonian of the spin system contains two main contributions. On one side we have the exchange interaction, characterized by an exchange constant $J$, between nearest neighbors that favor antiparallel arrangements. On the other we have a strong anisotropy energy that favors orientation in the axis towards the center of the triangles, this energy is characterized by an anisotropy constant $K$, and an anisotropy that penalizes the out-of-plane

orientations characterized by $K_z$. The resulting Hamiltonian becomes:

$$\mathcal{H} = J \sum_{\langle \mathbf{r},\mathbf{r}' \rangle} \mathbf{S}_\mathbf{r} \cdot \mathbf{S}_{\mathbf{r}'} - K \sum_{\mathbf{r}} \left( \mathbf{n}_\mathbf{r} \cdot \mathbf{S}_\mathbf{r} \right)^2 + K_z \sum_{\mathbf{r}} \left( \hat{\mathbf{z}} \cdot \mathbf{S}_\mathbf{r} \right)^2 , \tag{2.1}$$

where the anisotropy axis, $\mathbf{n}_\mathbf{r}$, are defined on each triangular element of the kagome lattice as illustrated on Fig.(2.1), and $\hat{\mathbf{z}}$ is the perpendicular axis to the plane. As the antiferromagnetic coupling favors configurations where all the moments in each triangle cancels one other, then if we consider any solid rotation of the moments in one triangle this condition stills. Following this idea we start from a given minimum (say, all spins pointing outward) and parameterize the configuration on any point in the lattice by a rotation matrix[44, 45]: $\mathbf{S}_\mathbf{r} = \mathcal{R}(\mathbf{r})\{\mathbf{n}_\mathbf{r} + a\left[\mathbf{L} - (\mathbf{L}\cdot\mathbf{n}_\mathbf{r})\mathbf{n}_\mathbf{r}\right]\}$, where $\mathbf{L}$ is the canting field assumed to be small. Restricting the description to the low energy structures we can assume the behavior of the rotation matrix $\mathcal{R}$ to be smooth, varying only across long length scales. Following [44] we write the Lagrangian of the system in terms of the variables $\mathbf{L}$ and $\mathcal{R}$ and express it within the smooth gradient approximation. We then proceed to solve the Euler-Lagrange equations for the field $\mathbf{L}$ finding:

$$T\mathbf{L} = \mathcal{R}^{-1}\partial_t \mathcal{R},$$

where $T_{\alpha\beta} = \delta_{\alpha\beta} - \frac{1}{3}\sum_{\mathrm{i}} n_{\mathrm{i}\alpha} n_{\mathrm{i}\beta}$. Replacing this solution into the action we are led to an effective Lagrangian density involving only the $\mathcal{R}$ field:

$$L = -\frac{\hbar^2}{2\sqrt{3}Ja^2}\mathrm{Tr}[(\mathcal{R}^{-1}\partial_t\mathcal{R})^2] - \mathcal{E}_{ex}(\mathcal{R}) - \mathcal{E}_{ani}(\mathcal{R}).$$

The anisotropy coupling favors two configurations, either all spins point toward the center of each triangle or away from it. This state of affairs leave us with two ground states that are degenerate and the main discussion that follow concerns mainly with magnetic textures that connect those states smoothly. In particular we focus on states that can be obtained from the uniform ground state by a smoothly varying rotation. It is a straightforward calculation to show that a gradient approximation of the exchange energy functional give us:

$$\mathcal{E}_{ex}[\mathcal{R}] = \frac{Ja^2}{2}\mathrm{tr}\left(g^{\mathrm{i}j}\mathcal{L}_\mathrm{i}\,\mathcal{L}_j\right)$$

where $\mathcal{L}_\mathrm{i} = \mathcal{R}^{-1}\partial_\mathrm{i}\mathcal{R}$ and $g^{\mathrm{i}j}_{\alpha\beta} = \mathrm{e}^\mathrm{i}_1\mathrm{e}^j_1 n^3_\alpha n^2_\beta + \mathrm{e}^\mathrm{i}_2\mathrm{e}^j_2 n^1_\alpha n^3_\beta + \mathrm{e}^\mathrm{i}_3\mathrm{e}^j_3 n^2_\alpha n^1_\beta$. In the last expression the vectors $\mathbf{e}_\mathrm{i}$ correspond to the ones defined in Fig. (2.1b). The anisotropy contribution to the energy is:

$$\mathcal{E}_{ani}[\mathcal{R}] = -K\sum_{\mathrm{i}}\left(n^\mathrm{i}\cdot\mathcal{R}n^\mathrm{i}\right)^2 + K_z\sum_{\mathrm{i}}\left(\hat{z}\cdot\mathcal{R}n^\mathrm{i}\right)^2.$$

## 2.3 Spin wave spectra

Now we proceed to analyze the spin wave spectra of the system around the ordered phase (Fig.2.2(a)). Here we call this phase just as homogeneous phase. To achieve this goal we describe the state of the system assuming that $\mathcal{R}$ is a rotation matrix made of Euler angles, $\mathcal{R}(\phi,\theta,\psi) = \mathcal{R}_{Z'}(\psi)\mathcal{R}_X(\theta)\mathcal{R}_Z(\phi)$. Calculating perturbations around the homogeneous phase

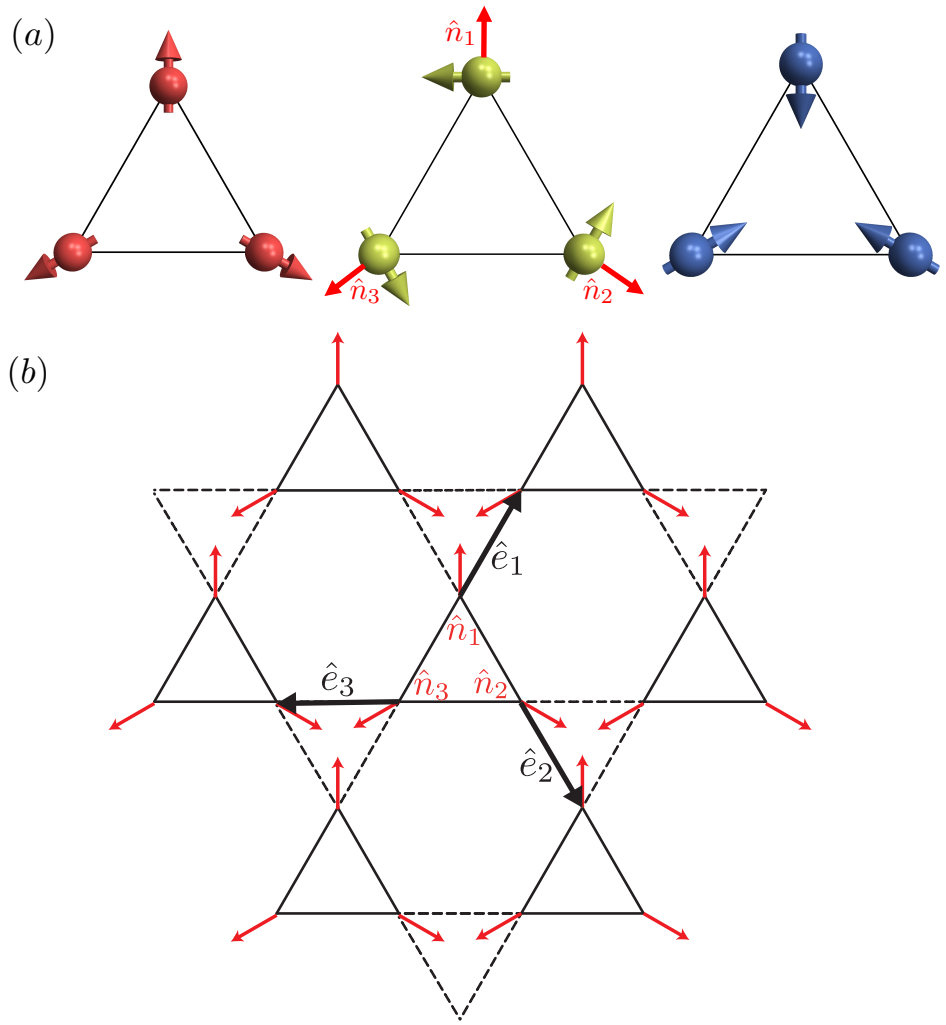


Figure 2.1: (a) Different configurations of a given triangle achieved through different rotations around the out of plane axes. An arbitrary configuration is encoded by a smooth distributions of such rotations. (b) Kagome lattice in the (111) plane in $Mn_3Ir$ where $Mn$ atoms are at each corner of a basis triangle. The basis vectors $\mathbf{n}_1 = (0, 1, 0)$, $\mathbf{n}_2 = (\sqrt{3}/2, -1/2, 0)$ and $\mathbf{n}_3 = (-\sqrt{3}/2, -1/2, 0)$ defined at every point in the lattice are shown. The vectors $\mathbf{e}_i$ point towards the nearest neighbours of each site. These vectors are used in the gradient expansion in the continuum approximation and are defined as $\mathbf{e}_1 = (\cos\pi/3, \sin\pi/3, 0)$, $\mathbf{e}_2 = (\cos\pi/3, -\sin\pi/3, 0)$, and $\mathbf{e}_3 = (-1, 0, 0)$.

we derive the effective action for the spin waves. As the perturbations are around the identity matrix, we found that the variables $\phi$ and $\psi$ correspond to the same rotation. Defining $\chi = \phi + \psi$ the equations of motion are:

$$\partial_t^2 \chi - \frac{3a^2 J^2}{\hbar^2} \nabla^2 \chi + \frac{12KJ}{\hbar^2} \chi = 0, \tag{2.2}$$

$$\partial_t^2 \theta + \frac{6J(K + K_z)}{\hbar^2} \theta = 0. \tag{2.3}$$

The spin wave spectra is split in a dispersion-less flat band with frequency

$$\omega^2 = \frac{6J(K + K_z)}{\hbar^2}$$

independent of the wave-vector and, a Klein-Gordon-like branch with frequency

$$\omega^2 = \frac{3a^2 J^2}{\hbar^2} k^2 + \frac{12KJ}{\hbar^2},$$

as is shown in Fig.2.2(b). In absence of anisotropy the spin wave branches become $\omega = 0$ and $\omega = vk$ with $v = \sqrt{3}aJ/\hbar$ in agreement with the results of [46, 47]. The presence of the flat band is a direct consequence of the absence of interlayer couplings within our model. If we consider interlayer exchange interaction including the terms outside the plane (111) in the gradient expansion, the flat band is modified as is shown in [40, 23, 48].

## 2.4 Soliton-like structures

We continue our discussion on magnetic textures looking at possible DWs in the order parameter field. We parameterize the rotation at each point by an angle $\phi$ and a rotation axis parallel to the $z$-axis (out of the plane). The Lagrangian density can be expressed in terms of $\phi$:

$$L = \frac{\hbar^2}{\sqrt{3}Ja^2} (\partial_t \phi)^2 - \sqrt{3}J \left(\nabla \phi\right)^2 + \frac{4\sqrt{3}K}{a^2} \cos^2 \phi.$$

This corresponds to the well known sine-Gordon model whose equation of motion is:

$$\partial_t^2 \phi - c^2 \nabla^2 \phi + \frac{m^2 c^4}{\hbar^2} \sin(2\phi) = 0$$

where we have defined the spin-wave velocity $c^2 = 3J^2 a^2/\hbar^2$ and the mass parameter $m^2 c^4/\hbar^2 = 6KJ/\hbar^2$. The solutions of this equation have been extensively studied[49]. Among its most celebrated solutions we can highlight stationary domain walls (where the angle travels all the way from zero to $\pi$) that are characterized by a domain wall width $W = a\sqrt{J/K}/2$. For $Mn_3Ir$ rough estimates of the parameters lead us to $W \sim$ 1-10$a$ [41]. The profile of the domain wall has a soliton-like form (Fig.2.3(b)):

$$\phi = 2 \tan^{-1}(\exp(x/W)).$$

To characterize the domain walls of we have solved numerically Landau-Lifshitz-Gilbert equation with an effective field derived from Eq.(2.1). By setting periodic boundary conditions

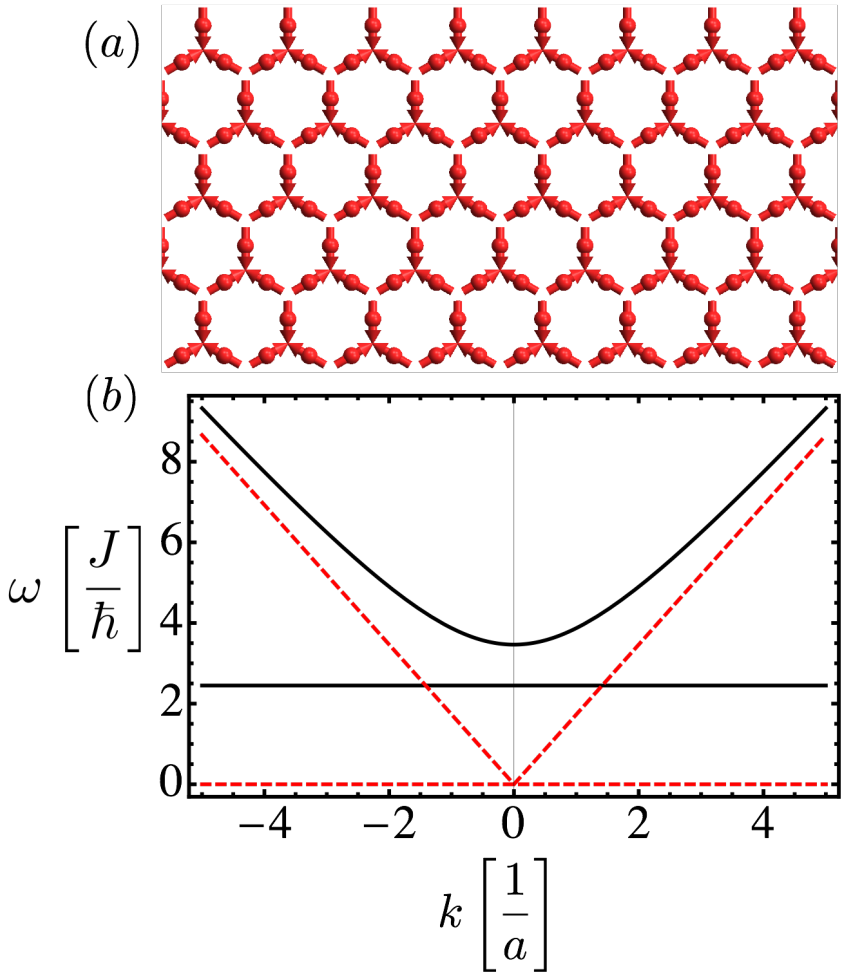


Figure 2.2: (a) Homogenous state with all the spins pointing toward the center of the triangles. This state is degenerated with the state with all the spins pointing away from the center of each triangle. (b) Dispersion relations for the spin wave spectrum of the homogeneous state. Solid lines correspond to the case with anisotropy and describe two branches one being a flat band with zero group velocity and another with a Klein-Gordon-like dispersion. Dashed line represent the dispersion relations of the isotropic case.

in the exchange field we have enforced a domain wall within our system and let the system to relax. The domain wall profile is then optimized and its width determined by fitting to a soliton like shape with adjustable width. The results are displayed in Fig.(2.3) and are in remarkable agreement with the long wave-length description of the continuum model.

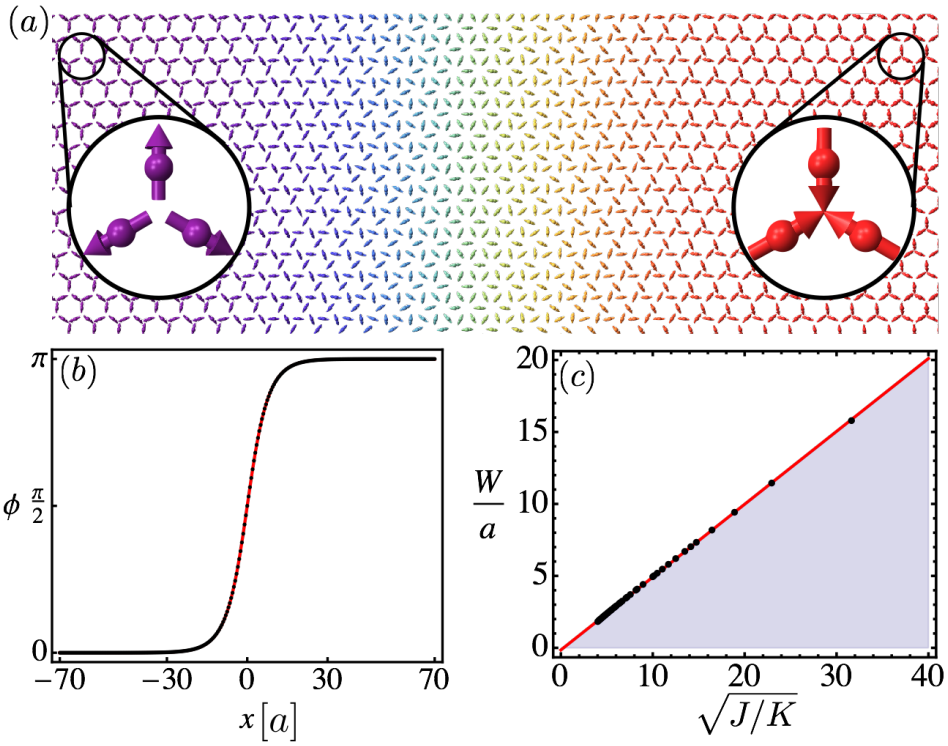


Figure 2.3: (a) Typical shape of a domain wall in kagome lattice. (b) Numerical fit of the soliton solution, black dots are the result of numerical simulation, red line corresponds to fitted solution $\phi = 2\tan^{-1}(\exp(x/W))$. (c) Width dependence on anisotropy. Black dots are numerical results while red dashed line is the fitted curve which has a slope equal to 1/2.

Along with the stationary domain walls just described the sine-Gordon model allows for mobile textures. As it is well known the profile of a domain wall moving with velocity $v$ is contracted by the Lorentz factor leading to a solution

$$\phi = 2\tan^{-1}(\exp[(x - vt)/W_0\sqrt{1-(v/c)^2}]).$$

We have verified this behavior using our simulations based on the Landau-Lifshitz equation. The results are shown in Fig.2.4.

Among the other localized excitations that are associated with the sine-Gordon equation, we have focused on the stationary breather solution [50],

$$\phi = 2\tan^{-1}\left[\sqrt{1-\omega^2}\cos(\omega t/\tau)/\omega\cosh(x\sqrt{1-\omega^2}/\lambda)\right],$$

where $\tau = \hbar/mc^2\sqrt{2}$, and $\lambda = \hbar/mc\sqrt{2}$. This solution represents a localized oscillation of the orientation of the local moments around the anisotropy axes. The numerical solution of the Landau-Lifshitz equation that is consistent with this state is shown in Fig.2.5(a)-(b).

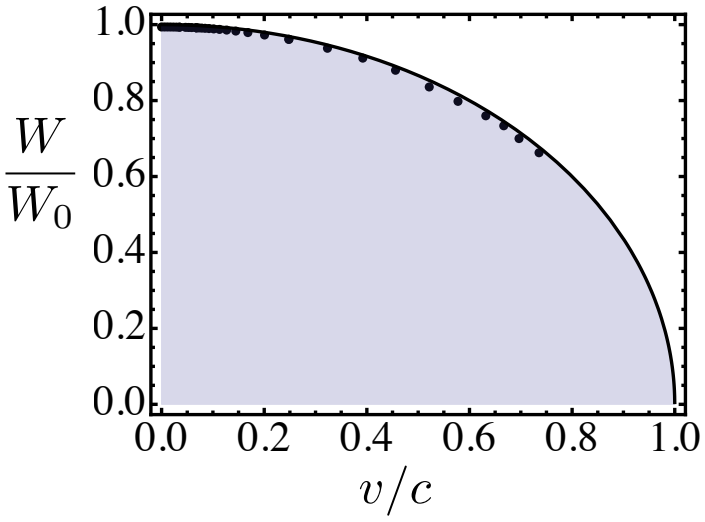


Figure 2.4: (a) Contraction of the width $W$ of a moving DW as function of speed $v$. The simulations were performed setting the easy axis anisotropy by $K = 0.025J$, and the hard axis anisotropy by $K_z = 0.1J$. The results of the Landau-Lifshitz equation shows perfect agreement with the Lorentz contraction factor $\sqrt{1-(v/c)^2}$, full line, that can be inferred from the sine-Gordon equation.

## 2.5 Topological defects

The topology of the order parameter space ($SO(3)$) opens a variety of possible topologically protected defects [51]. For example, the first homotopy group being $\pi_1(SO(3)) = \mathbb{Z}_2$, then we have two kinds of configurations. While textures which belong to class 0 can be continuously deformed to the uniform state, textures which belong to class 1 cannot. The latter are known as disgyrations in the context of $^3He$. The coalesence of two disgyrations generates a vortex-like trivial texture (as consequence of $1+1=0$). However, disgyrations have an energy that grows with system size then are not localized.

The second homotopy group of $\pi_2(SO(3))$ is trivial and skyrmions are not topologically protected. Nevertheless there are trivial stable solutions as the *lump* solution [50]. In Fig.2.6 we show examples of textures related with the previous topological properties.

Finally, the third homotopy group of the order parameter space is given by $\pi_3(SO(3)) = \mathbb{Z}$ which opens up the possibility of topologically stable point like defects. Physical realizations of this kind of topological defects have been studied in the context of superfluid $^3$He-A[52] and topological insulators[53]. Our description of a single kagome lattice needs to be extended to include interplane interactions in the gradient expansion. In this case the topological defect is a three-dimensional structure characterized by covering all possible rotations as we move away from its center. The winding number associated with the third homotopy group is given

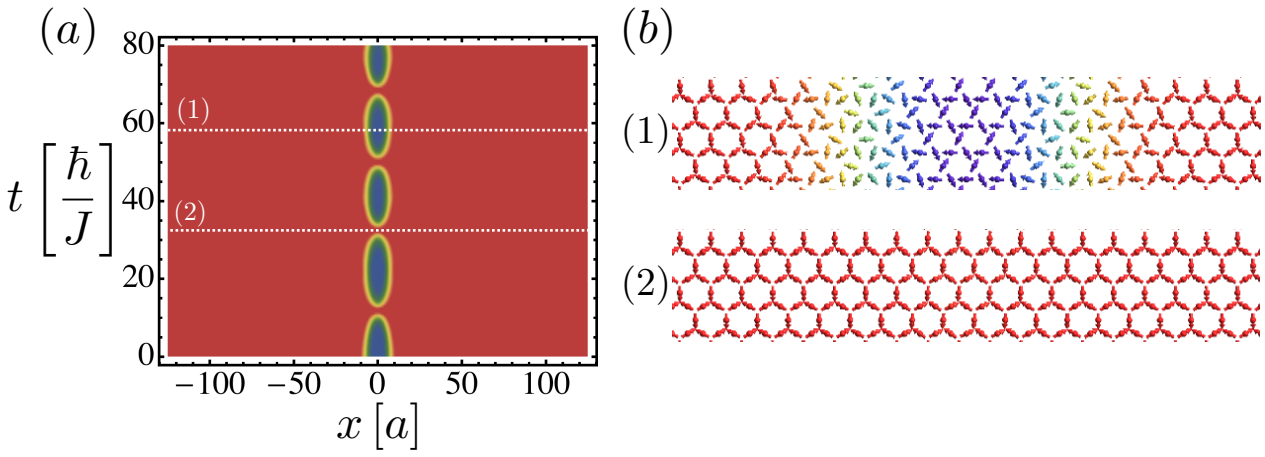


Figure 2.5: (a) Time evolution of the orientiation $\phi$ in the case of a breather state with frequency $\omega = 0.25$. The results correspond to the solution of the Landau-Lifshitz equation with the same paremeters as in Fig.2.4. The color code is the same as the one used for the DW. (b) Snapshot at time (1) and (2) showing the orientation of the local moments in the texture.

by[54, 55, 56]:

$$Q = \frac{1}{24\pi^2}\int \mathrm{d}r\ \varepsilon_{\mu\nu\lambda}\mathrm{tr}\left(\mathcal{L}_\mu\mathcal{L}_\nu\mathcal{L}_\lambda\right)$$

where $\varepsilon$ stands for the fully antisymmetric tensor. One possible realization of this kind of defects is the Shankar monopole[57]. The idea is to associate to each point of space $\vec{r} = r\hat{n}$ an operator that rotates around the $\hat{n}$-axis an angle $\chi(r)$. If $\chi$ is chose to go all the way from zero at the origin to $2\pi$ away from the monopole we can see that whole parameter space is covered twice. The texture so generated is stable under perturbations and becomes a finite energy topologically protected defect.

## 2.6 Conclusions

In this chapter we have addressed the behavior of textures in the order parameter field of non-collinear antiferromagnets. By pursuing a continuum description of the textures we have studied the spin-wave spectra around the homogeneous configuration and the behavior of domain walls. The spin wave spectra consists of two branches. One correspond to the usual Klein-Gordon-like dispersion relation while the other correspond to a flat band whose frequency is independent of the wave-number. Domain wall structure behave in a similar fashion than Bloch type domain walls in common ferromagnets with a characteristic with scaling with the square root of $J/K$ (exchange interaction compared with anisotropy). They are described by an effective sine-Gordon equation that allows us to predict the existence, along with stationary domain walls, of moving domain walls that travel undistorted across the system. We have compared the predictions of our continuum theory with the results of exact simulations of the Landau-Lifshitz-Gilbert equation and obtained a complete agreement. Finally we have discussed the topological defects that are allowed by the topology of the order parameter space.

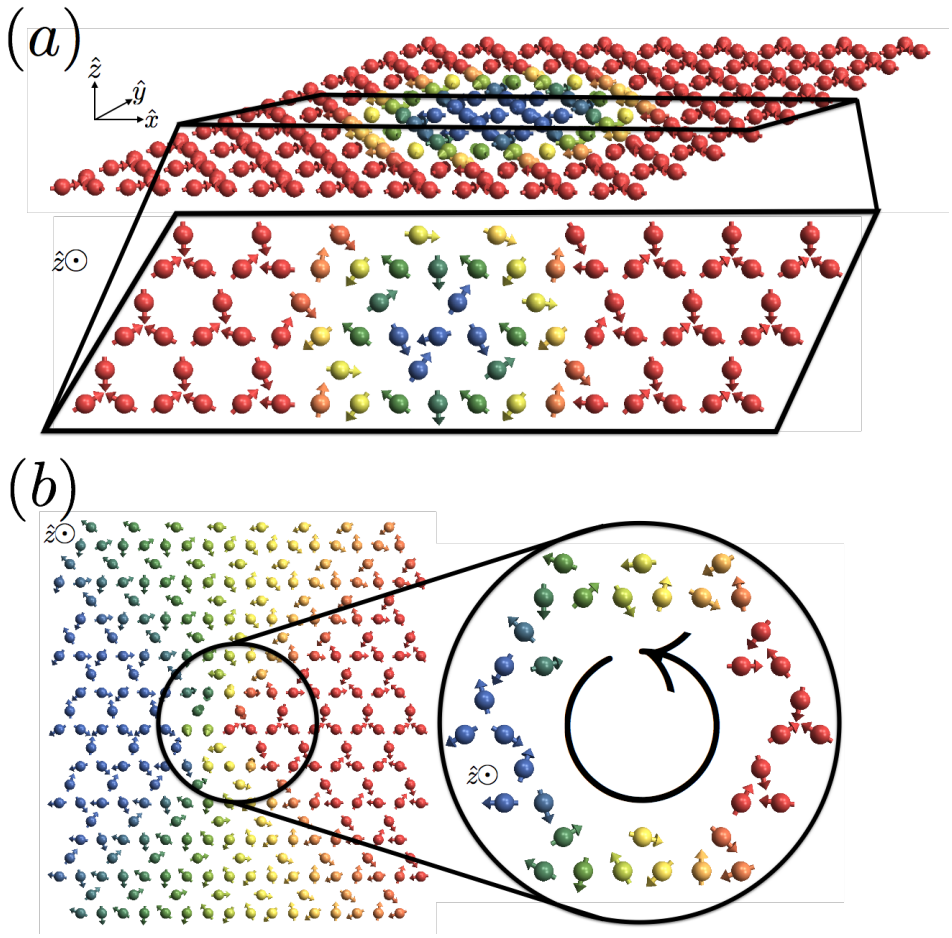


Figure 2.6: (a)Cartoon of a *lump* texture, given by the parameterization $\mathcal{R}(\eta, \hat{z})\mathbf{n_r}$, where $\eta(r) = 2\arctan[\exp\ (r-R)/W]$. This is an example of a trivial 2D texture. While this solution is stable, has no topological protection at all so it can be continuously deformed to the homogeneous state. (b) Cartoon of a class 1 disgyration. This solution is topologically protected because of the non-trivial homotopy $\pi_1(SO(3))$, then is not possible to reach the homogeneous state adiabatically. As this state is not localized, his energy grows with the size of the system.

# Chapter 3

# Antiferromagnetic magnonic crystal

In this chapter we describe the features of magnonic crystals based upon antiferromagnetic elements. Our main results are that with a periodic modulation of either magnetic fields or system characteristics, such as the anisotropy, it is possible to tailor the spin wave spectra of antiferromagnetic systems into a band-like organization that displays a segregation of allowed and forbidden bands. The main features of the band structure, such as bandwidths and bandgaps, can be readily manipulated. Our results provide a natural link between two steadily growing fields of spintronics: antiferromagnetic spintronics and magnonics. This work was developed in collaboration with Roberto Troncoso, Felipe Pesce and Álvaro Núñez, and it was published on December 17th of 2015 in Physical Review B.

## 3.1 Introduction

Small deviations of the local magnetization of a system can propagate coherently in the form of spin waves (SWs), whose associated quantum fields are known as magnons. Due to the lack of Joule heating associated with their transport they stand out as promising candidates for its application in the context of information processing[58, 59]. The field of solid state physics concerning the manipulation, detection and dynamics of the SWs in a magnetic system has been dubbed magnonics[60, 61, 62]. The field of magnonics has grown into a well established realm of magnetism and opened new paths in the understanding of magnetization dynamics of complex structures.

Most of the research in magnetism has focused on spin waves propagating across systems with an overall ferromagnetic order. For example, one of the most studied systems is Ytrium-Iron-Garnet(YIG) that, being ferrimagnetic, displays a net magnetic moment on each unit cell. A central theme in the field of magnonics is the implementation of magnonic crystals (MCs), the spin wave analog of photonic and plasmonic crystals, structures with magnetic properties spatially modulated in a periodic fashion. In a MC the spin wave spectra is organized in the form of bands with associated bandgaps that can be tailored by proper adjustment of the MC properties. A variety of magnonic devices have been proposed that profit from the spin waves as information carriers[63, 64, 65], signal filters, phase shifters,

isolators, and signal processing elements[60, 61, 62].

In this work we propose to use antiferromagnets (AF) as the basic background material in magnonics devices[1, 2]. To highlight the potential in the use of antiferromagnetic materials we illustrate two examples of magnonic crystals that can be implemented using antiferromagnetic elements. Among the main results we highlight the possibility of tailoring the magnonic bands by the use of modulations in the magnetic field, the anisotropy of the elements or simply by manipulating the geometry of the system. Our results point towards an effective engineering of the magnonic bands.

Antiferromagnetic based spintronics is a rapidly developing new field by its promising and unique properties for future spintronic devices in magnetism. Despite its lack of macroscopic magnetization, antiferromagnets, interact with spin-polarized currents and can give rise to spintronic effects such as magnetoresistance and spin transfer torques[13, 14, 15, 18, 19, 20, 21, 22, 66, 26, 27, 28, 30, 31], the piezo-spintronic effect[16] and skyrmion textures[67, 68] There are a number of advantages that AF systems present over ferromagnetic ones regarding potential applications. The lack of stray fields, rapid frequency switching in the terahertz range and its diverse functionalities to be integrated with ferromagnets, are among of the best qualities of antiferromagnets. The first one relates to the already mentioned lack of net magnetization. Due to this, they do not create magnetic fields which renders local all the interactions involved in its manipulation. Second, the typical time-scale associated with changes in the magnetic structure is several orders of magnitude shorter than the associated with ferromagnetic systems [69]. This opens a possibility to implement high-speed effects operating in the terahertz range. Finally, antiferromagnetism is observed more often and at much less demanding conditions than ferromagnetism, being found even in semiconductors at room temperature [70]. This allows us to envision hybrid devices that display features of both electronic and spintronic characteristics. Among the large assortment of antiferromagnetic materials, we have in mind those antiferromagnetic insulators with uniaxial anisotropy such as, for example, NiO[71], $MnF_2$[72, 73], $FeF_2$[74, 75]. Spin waves in AF have been studied since the dawn of quantum mechanics. Both from the theoretical point of view[76] as from the experimental one[77]. There is a great deal knowledge accumulated over decades involving the spectra of spin waves in a variety of AF. This opens a window of opportunity for effective control of the spin wave degrees of freedom. In this chapter, we work out, based on the phenomenological theory of spin dynamics in antiferromagnets developed by Hals et al. (Refs. [26, 27, 28, 30]), to account for the spin wave physics in spatially modulated antiferromagnets.

The structure of this chapter is the following. In Section 3.2, the phenomenological model for antiferromagnets is presented and the basic physics of spin waves in AF is discussed. The enquiry of AF magnonic bands, in Section 3.3, is considered in both scenarios either modulating periodically the anisotropy and external magnetic field.

## 3.2 Phenomenological theory

We start off our discussion by stating the basic features of our model. We study the dynamics of the staggered magnetization field in a spatially modulated antiferromagnet[26, 12, 78, 79].

In terms of the microscopic exchange energy, $J$, lattice constant $\ell$, coordination number $z$ and the uniaxial anisotropy $D$, the free energy density, $F$, for this system can be expressed[26, 27, 28, 30] as a functional of the staggered magnetization and magnetization fields, $\mathbf{n}$ and $\mathbf{m}$ respectively:

$$F = \left[\frac{a}{2}\mathbf{m}^2 + \frac{A}{2}\sum_{\mathrm{i}}(\partial_{\mathrm{i}}\mathbf{n})^2 - \frac{K_z}{2}\left(\mathbf{n}\cdot\hat{z}\right)^2 - \mathbf{H}\cdot\mathbf{m}\right], \tag{3.1}$$

where $a = 4zJS^2/\ell^3$, the homogeneous exchange energy; $A = zJS^2/2\ell$, the exchange stiffness; $K_z = 2DS^2/\ell^3$ the anisotropy (easy axis); and $\mathbf{H} = g\mu_B\mathbf{B}/\ell^3$ the external magnetic field. These parameters have spatial dependencies whose specific form will be specified later on. In $F$ the fields are further constrained to obey $\mathbf{n}\cdot\mathbf{m} = \mathbf{0}$ and $\mathbf{n}^2 = 1$ at every instant and everywhere within the system. The equations of motion can be obtained from a variation of the action where the constraints are enforced with the aid of suitable Lagrange's multipliers. The resulting dynamics is ruled by:

$$\dot{\mathbf{n}} = \gamma\mathbf{f}_m \times \mathbf{n}, \tag{3.2}$$

$$\dot{\mathbf{m}} = \gamma\left(\mathbf{f}_n \times \mathbf{n} + \mathbf{f}_m \times \mathbf{m}\right), \tag{3.3}$$

where:

$$\mathbf{f}_m = -a\mathbf{m} + \mathbf{n}\times\left(\mathbf{H}\times\mathbf{n}\right),$$

$$\mathbf{f}_n = A\mathbf{n}\times\left(\nabla^2\mathbf{n}\times\mathbf{n}\right) + K_z(\mathbf{n}\cdot\hat{z})\mathbf{n}\times\left(\hat{z}\times\mathbf{n}\right) - \left(\mathbf{n}\cdot\mathbf{H}\right)\mathbf{m},$$

and $\gamma$ is the effective gyromagnetic ratio.

To determine the spin waves we will consider small variations around the staggered magnetization (or Néel) vector and the canting field. The canting field $\mathbf{m}$ is small with respect to the local magnetic moment, which allows us to keep only first order term. Considering $\mathbf{n} = \mathbf{n}_0 + \delta\mathbf{n}(\mathbf{x}, t)$ and $\mathbf{m} = \mathbf{m}(\mathbf{x}, t)$ we expand up to first order the equations of motion (Eqs. (3.2) and (3.3)) as

$$\frac{\delta\dot{\mathbf{n}}}{\gamma} = -a\mathbf{m}\times\mathbf{n}_0 - \left(\mathbf{n}_0\cdot\mathbf{H}\right)\delta\mathbf{n}\times\mathbf{n}_0, \tag{3.4}$$

$$\frac{\dot{\mathbf{m}}}{\gamma} = A\nabla^2\delta\mathbf{n}\times\mathbf{n}_0 - K_z(\mathbf{n}_0\cdot\hat{z})^2\delta\mathbf{n}\times\mathbf{n}_0 - \left(\mathbf{n}_0\cdot\mathbf{H}\right)\mathbf{m}\times\mathbf{n}_0. \tag{3.5}$$

To solve these equations let us look for monochromatic waves in the form:

$$\delta\mathbf{n}(\mathbf{x}, t) = \left(\boldsymbol{\varepsilon}_1 n_1 + \boldsymbol{\varepsilon}_2 n_2\right)\mathrm{e}^{\mathrm{i}\mathbf{k}\cdot\mathbf{x} - \mathrm{i}\omega t}, \tag{3.6}$$

$$\mathbf{m}(\mathbf{x}, t) = \left(\boldsymbol{\varepsilon}_1 m_1 + \boldsymbol{\varepsilon}_2 m_2\right)\mathrm{e}^{\mathrm{i}\mathbf{k}\cdot\mathbf{x} - \mathrm{i}\omega t}. \tag{3.7}$$

In this representation we have used the constraints to express both fluctuating fields in the plane perpendicular to $\mathbf{n_0}$ that is spanned by the mutually orthogonal (but otherwise arbitrary) vectors $\boldsymbol{\varepsilon}_1$ and $\boldsymbol{\varepsilon}_2$. In this expression $n_{1,2}$ and $m_{1,2}$ are complex coefficients. Starting from Eqs. (3.4-3.7) in a direct way we can assess the problem of spin waves in a homogeneous antiferromagnet. The results are, naturally, consistent with the well-known dispersion relation[79]

$$(\omega \pm \gamma H)^2 = a\gamma^2(Ak^2 + K_z). \tag{3.8}$$

As can be seen in Fig. 3.1 there are two independent solutions. One has a phase difference between $n_1$ and $n_2$ equal to $\pi/2$, while the other has a phase difference equal to $-\pi/2$. These solutions correspond, therefore, to spin waves circularly polarized to the left and to the right. In the absence of magnetic field both branches are degenerated. This degeneracy is split by the magnetic field that shifts the dispersion relation of the right-polarized waves upward and the dispersion relation of the left-polarized waves downward by an equal amount $\gamma H$. An

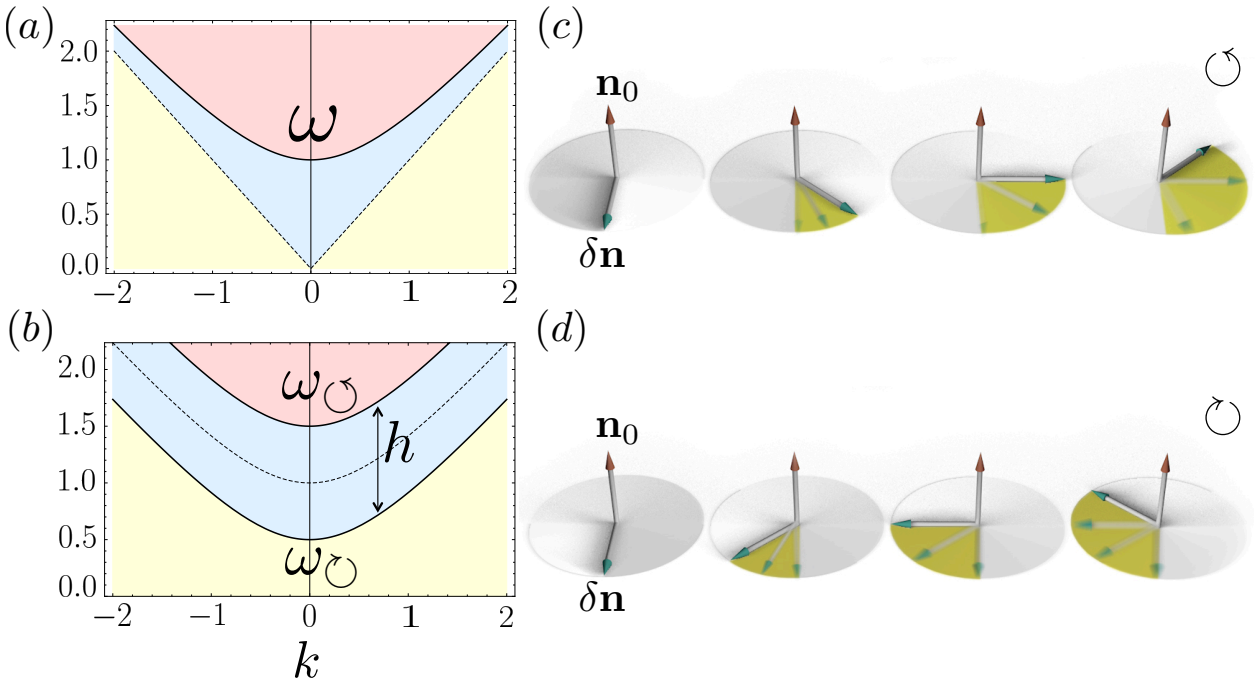


Figure 3.1: (a) Spin wave dispersion relation for the homogeneous antiferromagnet. Without anisotropy the relation is dispersionless (dashed line). Addition of anisotropy raises a gap and changes the dispersion relation to the Klein-Gordon form (full line). In both cases the dispersion relation is doubly degenerated reflecting the two possible polarizations of the spin wave. (b) Addition of a homogeneous magnetic field splits the degeneracy and creates different dispersion relations ($\omega_{\circlearrowleft}$ and $\omega_{\circlearrowright}$) for the two opposite polarizations. (c) and (d) Illustration of the two polarizations for the spin wave. The disturbance is perpendicular to the equilibrium staggered magnetization vector ($\mathbf{n}_0$) and precesses in a clockwise or anti-clockwise sense.

important aspect of the spin wave spectra that is encoded by Eqs. (3.4) and (3.5) is that oscillations in the staggered magnetization order parameter $\delta\mathbf{n}$ are linked to oscillations in the magnetization. In fact, a quick look at Eqs. (3.4) and (3.5) allows us to write:

$$\mathbf{m} = -\frac{1}{a}\left(\frac{1}{\gamma}\mathbf{n}_0 \times \delta\dot{\mathbf{n}} + (\mathbf{n}_0 \cdot \mathbf{H})\delta\mathbf{n}\right). \tag{3.9}$$

This simple result is of the great importance since it provides a way to excite and measure antiferromagnetic spin waves by coupling them to the oscillation in the magnetization field that they carry. This coupling to the magnetic degrees of freedom has been used for decades to characterize the spin wave spectra of antiferromagnets[80, 81]. In this way it is possible to use magnetization probes, such as Faraday's and Kerr's effects or Brillouin light scattering[60,

61, 62], of widespread usage in the field of magnonics, to control and study antiferromanetic spin waves.

## 3.3 Antiferromagnetic spin wave bands

Now we are ready to present the main result of the work, the study of different ways in which these antiferromagnetic spin waves can be manipulated with the aid of periodic manipulation of the system parameters. We will see how this manipulation gives rise to magnonic bands that can be tailored with precision. There are basically two essentially different ways to control the antiferromagnetic spin waves. Starting from Eqs. (3.2) and (3.3) we note the possibilities of modulating the system parameters (exchange constants, anisotropy, etc) or the magnetic field. Both parameters can be modulated to generate magnonic crystals and in what follows we will study the peculiarities of each particular modulation.

Eliminating $\mathbf{m}$ from the equations of motion we are led to the following wave equation:

$$\delta\ddot{\mathbf{n}} = \nabla^2\delta\mathbf{n} - \kappa\ \delta\mathbf{n} + 2h\ \delta\dot{\mathbf{n}} \times \mathbf{n}_0 + h^2\delta\mathbf{n}, \tag{3.10}$$

where we have set $\tau = 1/\sqrt{K_z a\gamma^2}$ as the unit of time and $\lambda = \sqrt{A/K_z}$, the domain wall width, as the unit of length. In the last equation $\kappa$ and $h$, the dimensionless anisotropy coefficient and $h$ and dimensionless magnetic field ($h = \gamma\tau(\mathbf{n}_0 \cdot \mathbf{H})$) respectively, are regarded as periodically modulated. For common antiferromagnets[72, 74, 82] the value of $\tau$ and $\lambda$ lie in the range of picoseconds and a few nanometers respectively.

The solutions to the wave equation under a periodic modulation can be expressed in the form of Bloch wave functions $\delta\mathbf{n}(\mathbf{x}, t) = \mathrm{e}^{\mathrm{i}\mathbf{k}\cdot\mathbf{x}-\omega t}(\boldsymbol{\varepsilon}_1 n_1(\mathbf{x}) + \boldsymbol{\varepsilon}_1 n_2(\mathbf{x}))$ where $n_1(\mathbf{x})$ and $n_2(\mathbf{x})$ are periodic functions with the same period as the spatial modulation. The equation of motion, within the Bloch's representation, unfolds into two coupled equations for $n_1(\mathbf{x})$ and $n_2(\mathbf{x})$ that can only be fulfilled by choosing a $\pm\pi/2$ phase-shift between them. The waves are, therefore, circularly polarized as in the homogeneous case. Due to the magnetic field there is a splitting between the two circular polarizations. For right polarized waves we have $\delta\dot{\mathbf{n}} \times \mathbf{n}_0 = \omega\delta\mathbf{n}$ while for left polarized waves we have $\delta\dot{\mathbf{n}} \times \mathbf{n}_0 = -\omega\delta\mathbf{n}$. The equation of motion becomes:

$$-\omega^2\delta\mathbf{n} = \nabla^2\delta\mathbf{n} - \kappa\delta\mathbf{n} \pm 2\omega\ h\delta\mathbf{n} + h^2\ \delta\mathbf{n}, \tag{3.11}$$

where the $\pm$ sign is fixed by the polarization of the spin wave. This equation, with $\kappa$ and $h$ regarded as periodic functions of space, is the main tool to describe a spin wave crystal within an antiferromagnet. Let us give two examples of antiferromagnetic magnonic crystals that use this equation as the starting point.

### 3.3.1 Periodically modulated anisotropy

We begin our discussion by considering the problem in absence of magnetic field. We will focus on an one-dimensional array with spatially modulated anisotropy as illustrated in Fig. (3.2). When modulating the spatial anisotropy one can expect that the exchange parameters,

$a$ and $A$, should also be modified. Our theory is capable to handle those modulations in a straightforward manner. However, to avoid clumping our discussion with far too many parameters we will focus in a model problem where only the anisotropy is modulated. We have, then, a series of slabs of width $\beta$ with different anisotropies are arranged with period $\alpha$. Spin waves that propagate along direction transverse to the slabs experience a periodic modulation of the anisotropy parameter thereby giving rise to magnonic bands. This situation can be modeled by the equation

$$\delta\ddot{\mathbf{n}} = \nabla^2\delta\mathbf{n} - \kappa(y)\delta\mathbf{n}, \tag{3.12}$$

which shows complete degeneracy for the different polarizations. Searching for plane waves along the $x$ direction, with wave number $k_x$, we find

$$(\omega^2 - k_x^2)\delta n_\pm = -\frac{\mathrm{d}^2}{\mathrm{d}y^2}\delta n_\pm + \kappa(y)\delta n_\pm. \tag{3.13}$$

In the physical problem at hand the anisotropy is modulated in a piece-wise constant fashion. The background anisotropy of the system is chosen as the basis for the dimensionless anisotropy $\kappa$. There are slabs of width $b$ distributed uniformly with period $a$, and within these the anisotropy is $1 + \delta\kappa$. This problem is equivalent to a Schrödinger equation with periodic piece-wise constant potential that lead us to the well-known Kronig-Penney model for electrons. Solutions of this model can be found in textbooks[83] and consist of the matching of solutions at each side of the structure and imposing Bloch-boundary conditions. In Fig. 3.2 we present the results for a variety of system parameters. A glance at Fig. 3.2 allows us to state the main results that are (a) double degenerated band structure in account for different polarizations; (b) the appearance of forbidden energies bands; and, (c) the appearance of bands of allowed energies with characteristic bandwidths. As shown in the Fig. 3.2d those features can be controlled by an appropriate selection of the parameters of the magnonic crystal. The band structure can be further controlled by exposing the system to the effects of a magnetic field that results in a splitting of the degeneracy of the bands. This is shown in Fig. 3.2c.

### 3.3.2 Field mediated magnonic crystal

We now consider a magnonic crystal mediated by magnetic field. In this system a two dimensional antiferromagnet is exposed to a periodically modulated external magnetic field. While the details of the generation of this magnetic field are irrelevant for the conclusions we are going to draw, we can picture the following arrangement: locate the antiferromagnetic system underneath a periodic array of wires as depicted in Fig. 3.3a. The situation that we propose consists on having a current propagating across the wires. The magnitude of the current across each wire is constant while the direction of the current is changed between consecutive wires. This type of arrangement has been proposed and studied experimentally in Ref. [84] to the design of current-controlled magnonic crystals. In this way the Oersted field generated by the array of wires acts on the antiferromagnet in the form of a spatially periodic magnetic field that enters into the wave equation (Eqs. (3.4-3.5)). To fix ideas on

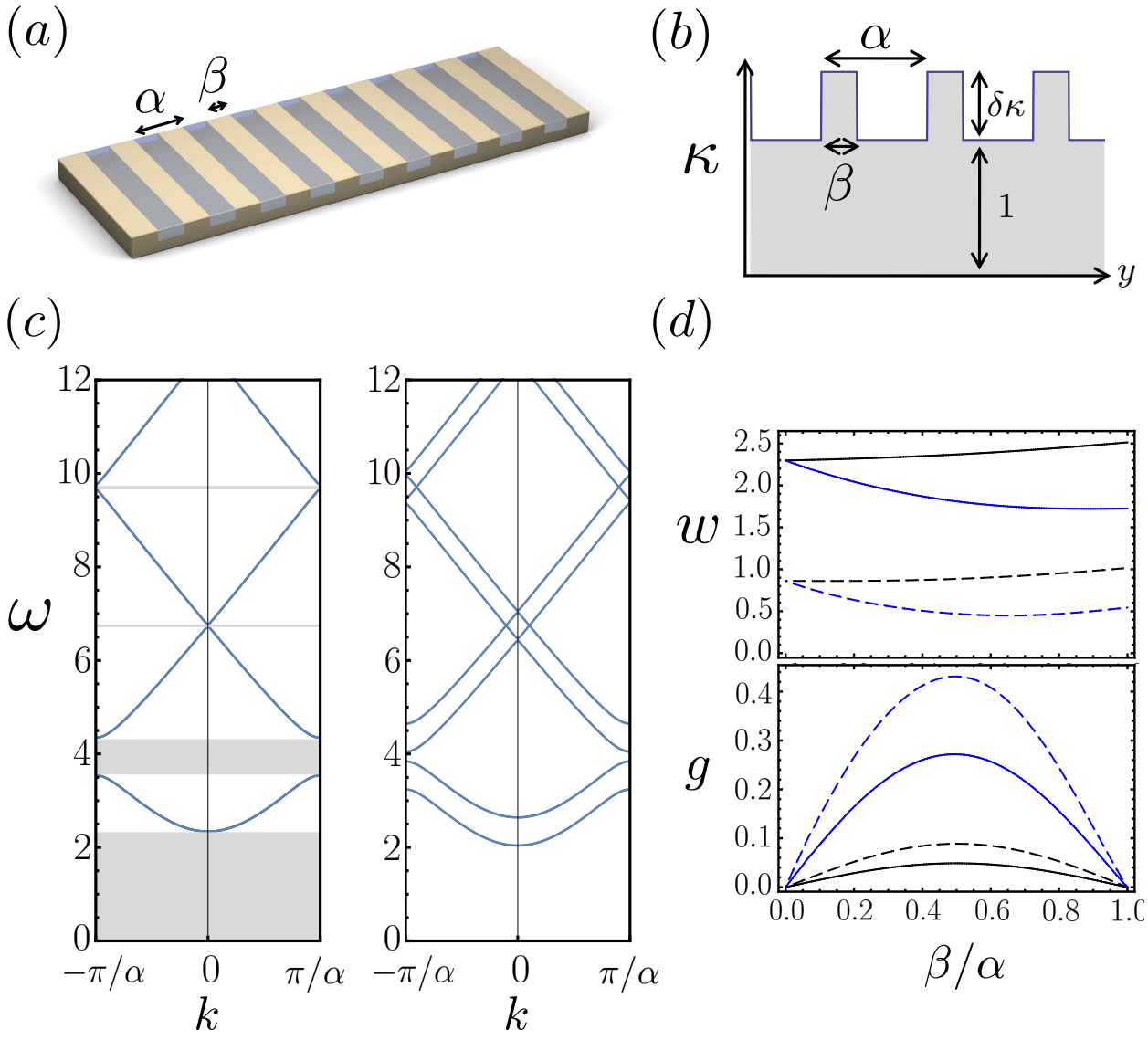


Figure 3.2: (a) Model system for a magnonic crystal, a heterostructure with changing anisotropy, illustrating the geometric features. (b) Simple effective potential that represents the effect of the modulated anisotropy. With the choice of units given in the text, the potential is characterized by a reference anisotropy equal to unity and deviations from it equal to $\delta\kappa$. (c) Left: Magnonic dispersion relation for $\alpha = 1.0$, $\beta = 0.5$ and $\delta\kappa = 10$. Bands are doubly degenerated in account for the different polarizations. Bands of forbidden frequencies are highlighted. Right: Same situation under the action of a uniform magnetic field $h = 0.3$. The degeneracy between the different polarization states is broken. (d) Some features of the band structure are displayed as a function of $\beta/\alpha$. Top: Bandwidth of the first bands is displayed for different values of the crystal, full lines correspond to $\alpha = 1$ and dashed lines to $\alpha = 2$. The black and blue lines correspond to $\delta\kappa = -0.5$ and $\delta\kappa = 3.0$ respectively. Bottom: With the same parameters we display the bandgap between the first and second bands.

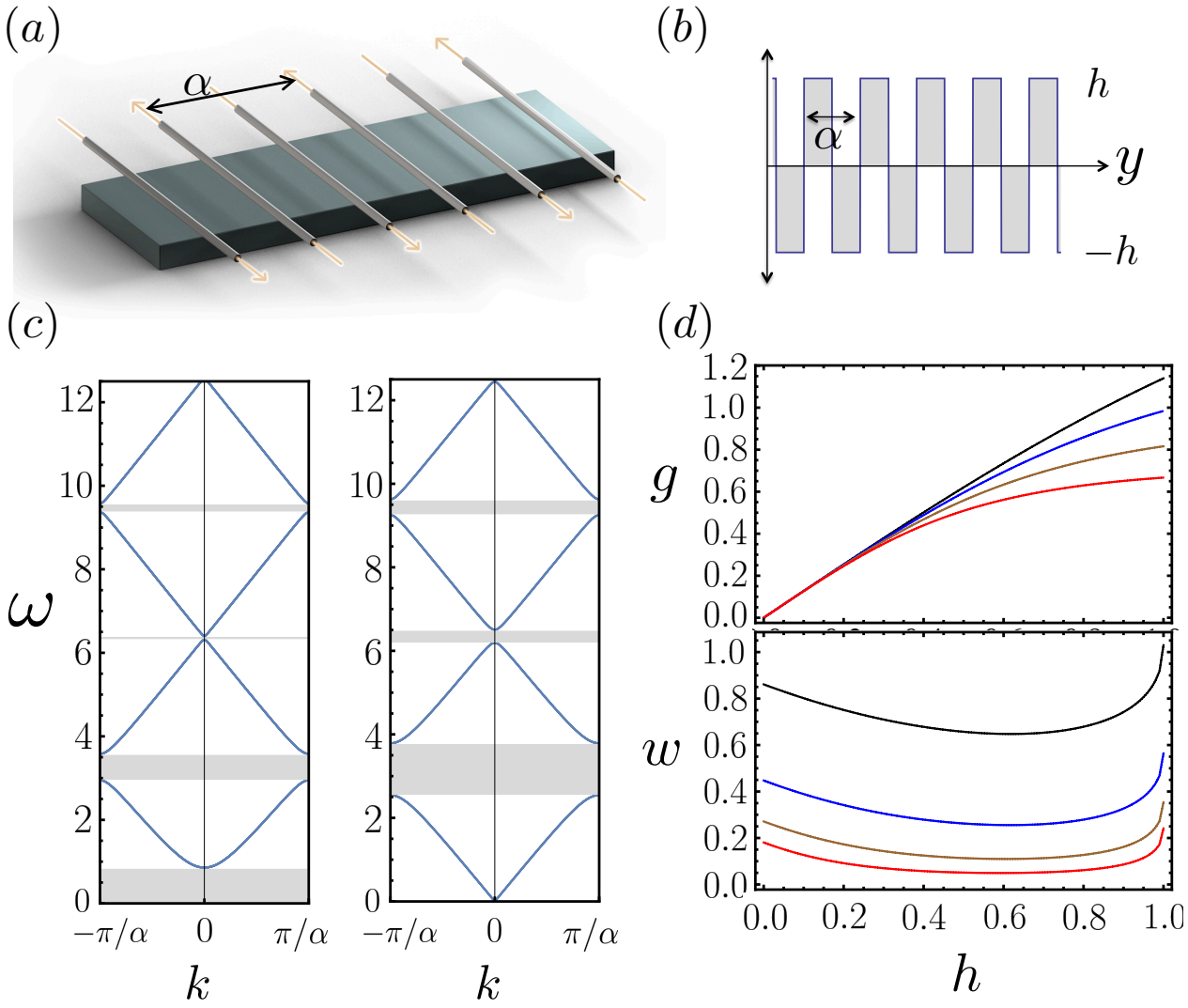


Figure 3.3: (a) Arrangement of wires on top of a two-dimensional antiferromagnetic sample. The magnetic field they generate form a magnonic crystal; (b) The system is characterized by spatially modulated magnetic field that oscillates between two extrema $\pm h$ within a period $\alpha$; (c) Left: band structure for $\alpha = 1$ , $\kappa = 1$ and $h = 0.5$. Right: Band structure for $h = \kappa = 1$. The lowest band minimum reaches zero, signaling the spin-flop instability; (d) As a function of the magnetic field strength we display the band structure parameters. Top: The band gap for $\alpha = 2$, 3, 4, and 5; Bottom: band width of the first band for the same parameters.

the nature of this equation we approximate the field by a piece-wise constant behavior with values $\pm h$. Assuming a plane wave behavior along the $x$-direction we find

$$(\omega^2 - k_x^2 + \kappa + h^2)\delta n_\pm = -\frac{\mathrm{d}^2}{\mathrm{d}y^2}\delta n_\pm \pm 2h\omega\delta n_\pm. \tag{3.14}$$

This problem is solved following the standard procedure described in [83], in the same way as our previous discussion. The main results are displayed in Fig. 3.3. The periodic magnetic field gives rise to a band structure with characteristic bandgaps and bandwidths that are characterized in Fig. 3.3d. As we increase the strength of the magnetic field, the lowest point in the first band decreases continuously from the value at zero field. This trend leads to an instability at $h = \sqrt{\kappa}$ when the lowest band touches the bottom of the axis. For fields greater than this critical value the ground state is distorted in what is known as the spin-flop transition[80, 81].

## 3.4 Conclusions

We have discussed the possibility of implementing magnonic crystals in the context of antiferromagnetic spintronics. We proposed two complementary methods to achieve control over the magnonic degrees of freedom: first by controlling the anisotropy properties of the spin wave system and second by exposing the antiferromagnet to a periodically modulated magnetic field. In both cases we discussed quantitatively the properties of the resulting spin wave spectra and showed how it led to a band-like structure of allowed and forbidden bands whose quantitative features can be tailored by proper adjustment of the parameters of the magnonic crystal. This proposal bridges together the two rapidly developing fields of magnonics and antiferromagnetic spintronics.

# Chapter 4

# Piezospintronic effect

The generation and detection of pure spin currents has been one of the main goals of spintronics. One of the most promising effects for this purpose is the inverse spin-Hall effect (ISHE). In this chapter we propose a possible path to generate pure spin currents by applying strain under a material with specific symmetry properties. This work is a direct application of the theory developed by A. S. Núñez [16] for the piezospintronic effect. Along this chapter we present a brief summary of the named theory and then show the piezospintronic response of antiferromagnetic graphene and antiferromagnetic zinc-blende structures. This work has been developed in collaboration with A. S. Núñez, and R. E. Troncoso and it is not published yet.

## 4.1 Introduction

The intuitive notion of spin current is based on the idea of different spin species flowing at different speeds. This notion, in the context of quantum mechanics, is a good notion only in systems where the spin is a well behaved quantum number. If the spin is not conserved, such as for example when one electron is under the effect of the spin orbit interaction, the problem of the definition of a spin current is subtle. Along this chapter we will use the definition of spin current given by [85]

$$\mathbf{J}^{S}_{\mathrm{i};j} = \frac{\mathrm{d}\left(\hat{S}_{\mathrm{i}}\hat{R}_{j}\right)}{\mathrm{d}t}, \tag{4.1}$$

where $\hat{R}$ correspond to the electronic position operator. This definition has several advantages, for example when the spin is a conserved quantity from Eq. (4.1) emerges naturally the intuitive notion of spin current,

$$\mathbf{J}^{S}_{\mathrm{i};j} = \hbar(\mathbf{v}_{\uparrow} - \mathbf{v}_{\downarrow})_{j}, \tag{4.2}$$

where $\mathbf{v}_{\uparrow}$ ($\mathbf{v}_{\downarrow}$ ) represents the velocity of the spin up (down) carriers. Additionally , this definition relates the spin current to the time derivative of the spin dipolar moment $\mathbf{P}^{S}_{z;j}$, which will be used in the following sections.

## 4.2 Analysis of the direct and converse piezospintronic effect

With the precise definition of a spin current we proceed to analyze the basic symmetry requirements imposed on the system in order to have a no null piezospintronic effect. Let us suppose that under strain a spin current is generated in a generic system. The spin dipole moment should be expected to satisfy (in a linear regime) an equation

$$\mathbf{P}^{S}_{\mathrm{i};j} = \lambda_{\mathrm{i};j,kl}\mathbf{u}_{kl}. \tag{4.3}$$

Equation (4.3) is a direct analogy with the piezoelectric effect and is the definition of the piezospintronic tensor $\lambda$. In it $\mathbf{u}_{kl} = (\partial_k u_l + \partial_l u_k)/2$ is the strain tensor[86], where $u$ is the deformation field, and $\mathbf{P}^{S}_{\mathrm{i};j}$ is the spin dipole moment generated by the deformation of the system. The element $\lambda_{\mathrm{i};j,kl}$ must be understood as the relation of a spin current in direction $j$ of spins oriented in i, with a strain in direction $kl$. Since the spin dipole moment is a pseudo-tensor $\lambda$ must be a pseudo-tensor. Under an inversion transformation $\mathbf{x} \to -\mathbf{x}$, $\lambda$ must change sign. It is important to say that time reversal symmetry breaking is required for a crystal in order to show a piezospintronic effect.

Let us call by $\mathcal{R}$ and $\mathcal{I}$ the time reversal and the spatial inversion operations. Materials which are invariant under the consecutive action of $\mathcal{R}$ and $\mathcal{I}$ can not have a piezoelectric response under strain. This is because the current generated for the different spin species cancel each other. Then, crystals with $\mathcal{R}$ and $\mathcal{I}$ broken symmetries but invariants under $\mathcal{RI}$ (or $\mathcal{IR}$) will generate a pure spin current under an external strain.

The thermodynamic conjugate of the spin current, a spin force, was identified in [85]. The relationship between the spin current and the spin force allows us to state that a converse piezospintronic effect is manifested in a system that already manifests a direct piezospintronic response. From Onsager's relations[87] a stress is expected in response to a spin current injected into the system:

$$\sigma_{\mathrm{i}j} = \tilde{\lambda}_{l;m,\mathrm{i}j}\mathbf{J}^{S}_{l;m}, \tag{4.4}$$

where $\sigma$ stands as the stress tensor in response to the spin current $\mathbf{J}^S$. This converse effect might lead to novel mechanism to detect pure spin currents.

## 4.3 Microscopic theory of the piezospintronic effect

With the symmetry requirements that are necessary for a system to display the piezospintronic effect we proceed to explain how the piezospintronic response might be calculated. A convenient interpretation of Eq. (4.1) arises from the Berry phase theory of polarization [88, 89, 90, 91, 92, 93]. Instead of calculate the spin current directly, we evaluate it in terms of changes of spin current associated with an adiabatic deformation and then use the whole toolbox for adiabatic processes of quantum mechanics. We parametrize the elastic strain by some parameters $Q$. Then we consider the strain tensor as function of $Q$, $u_{kl} = u_{kl}(Q)$, as

well the Hamiltonian $\mathcal{H} = \mathcal{H}(Q)$. The change in spin dipolar moment density in response to an adiabatic change in the external parameters $Q \to Q + \mathrm{d}Q$, is

$$\mathrm{d}\mathbf{P}^S_{\mathrm{i};j} = \mathbf{A}^{\mu}_{\mathrm{i};j}\mathrm{d}Q_{\mu}, \tag{4.5}$$

where

$$\mathbf{A}^{\mu}_{\mathrm{i};j} = -\sum_{\nu}\int \frac{\mathrm{d}^{\mathrm{d}}k}{(2\pi)^{\mathrm{d}}} n_{\nu}(k)\mathrm{Im}\left\langle \frac{\partial\phi_{\nu}}{\partial k_j}\right| \hbar\sigma_{\mathrm{i}} \left|\frac{\partial\phi_{\nu}}{\partial Q^{\mu}}\right\rangle . \tag{4.6}$$

These equations are analogous to the ones used in the theory of polarization [93]. The main difference is the presence of the Pauli matrix in between the brackets. This difference make the set of Eqs. (4.6) appropriate to evaluate changes in spin dipolar moments instead of changes in polarization. Eqs. (4.5) and (4.6) allows us to calculate the piezospintronic response of any material. Then the piezospintronic response is calculated by performin an integration of Eq. (4.5) over a path $\Gamma$ in parameter space ($Q$) which the system is swept under the application of an external strain

$$\delta\mathbf{P}^S_{\mathrm{i};j} = \int_{\Gamma} \mathbf{A}^{\mu}_{\mathrm{i};j}\mathrm{d}Q^{\mu}. \tag{4.7}$$

The left hand side of Eq. (4.7) stands for the accumulated spin dipolar moment during the process of distorting the system from a reference configuration. Changes in the configuration are accompanied by pure spin currents as we have non-zero $\delta\mathbf{P}^S$. Following Eq. (4.1), the rate of change of $\mathbf{P}^S$ with time corresponds to the spin current $\mathbf{J}^S = \mathrm{d}\mathbf{P}^S/\mathrm{d}t$. The change in the expectation value of the operator $\mathbf{P}^S$ can be calculated using the Kubo formula

$$\mathrm{d}\mathcal{A}_{\mu} = \mathrm{Im}\left(\mathrm{i}\hbar\sum_{\nu\neq\mu}\frac{\langle\psi_{\mu}|\,\mathbf{P}^S\,|\psi_{\nu}\rangle\,\langle\psi_{\nu}|\,\mathrm{d}\mathcal{H}\,|\psi_{\mu}\rangle}{(E_{\mu}-E_{\nu})^2}\right). \tag{4.8}$$

Standart matrix manipulations [85] leads to Eqs. (4.5) and (4.6).

Now we proceed to illustrate these ideas calculating the piezospintronic response of two interesting materials: antiferromagnetic graphene and antiferromagnetic zinc-blende.

## 4.4 Piezospintronic response of antiferromagnetic graphene

We consider an antiferromagnetic honey-comb lattice with staggered magnetization. Different sub lattices have different spin species that are given by $\Omega_{\mathrm{i}} = \Delta\hat{z}$ if site i belongs to one sub lattice (let's say A) and $\Omega_{\mathrm{i}} = -\Delta\hat{z}$ if site i belongs to the other sub lattice (B). Under inversion around the center of the unit cell the role of sub lattices is reversed, it does not have inversion symmetry. Also if we consider a spin inversion (time reversal) the role of sub lattices is reversed again. Then after consecutive inversion $\mathcal{R}$ and time reversal $\mathcal{I}$, the system is unchanged, i.e. is invariant under $\mathcal{RI}$. Therefore we expect a pure piezospintronic effect.

Besides the local exchange term we complement our model with the hopping amplitudes to first nearest neighbours. These amplitudes are $t_1$, $t_2$, and $t_3$ for the links $\vec{\delta}_1$, $\vec{\delta}_2$, and $\vec{\delta}_3$ respectively (see Fig. 4.4).

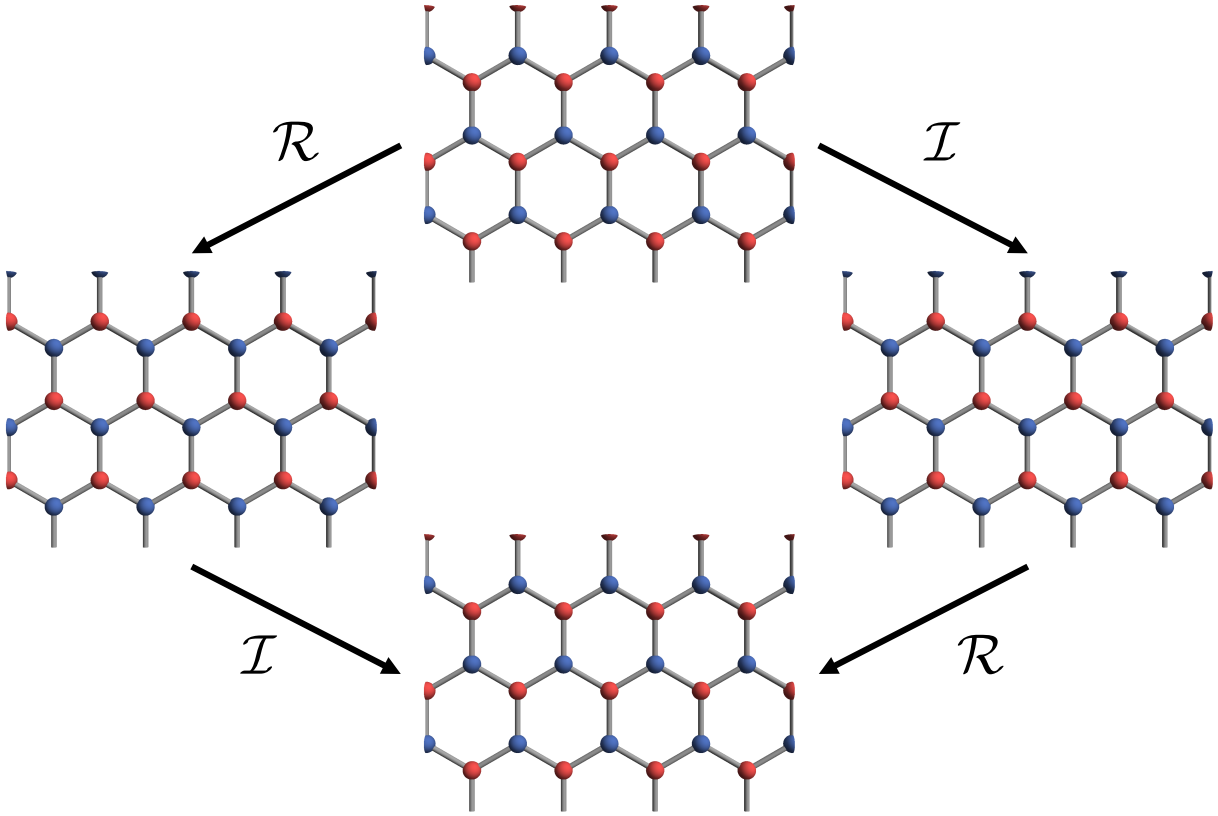


Figure 4.1: Symmetry analysis of honey-comb (graphene) lattice with two different sub lattices which stand in this case for two different spin species, for instance red spheres represent a spin up, and blue spheres a spin down. It is direct to see that spatial inversion ($\mathcal{I}$), and time reversal ($\mathcal{T}$) symmetries are broken, then the system is not allowed to present a piezoelectric effect. $\mathcal{TI}$ (or $\mathcal{IT}$) symmetry instead is preserved instead, then we expect the system to develop a pure piezospintronic effect.

The net Hamiltonian is

$$\mathcal{H} = -\sum_{\langle \mathrm{i},j\rangle,\sigma} t_{\mathrm{i}j}\left(c^{\dagger}_{\mathrm{i}\sigma}c_{j\sigma} + h.c\right) + \Delta\sum_{\mathrm{i}\sigma\sigma'}(-1)^{\mathrm{i}}c^{\dagger}_{\mathrm{i}\sigma}\tau^{z}_{\sigma\sigma'}c_{\mathrm{i}\sigma'}, \tag{4.9}$$

where $c^{\dagger}_{\mathrm{i}\sigma}$ is the operator that creates an electron with spin $\sigma$ on the site i, $t_{\mathrm{i}j}$ is the hopping amplitude to go from site i to site $j$, $\Delta(-\Delta)$ is the local energy associated with spin up(down) species. This Hamiltonian in momentum representation is

$$\mathcal{H}_{\uparrow\uparrow} = \begin{pmatrix} \Delta & \gamma_k \\ \gamma^*_k & -\Delta \end{pmatrix}; \qquad \mathcal{H}_{\downarrow\downarrow} = \begin{pmatrix} -\Delta & \gamma_k \\ \gamma^*_k & \Delta \end{pmatrix}, \tag{4.10}$$

where $\gamma_k = \sum_{\mathrm{i}} t_{\mathrm{i}} \exp(\mathrm{i}\vec{k}\cdot\vec{\delta}_{\mathrm{i}})$.

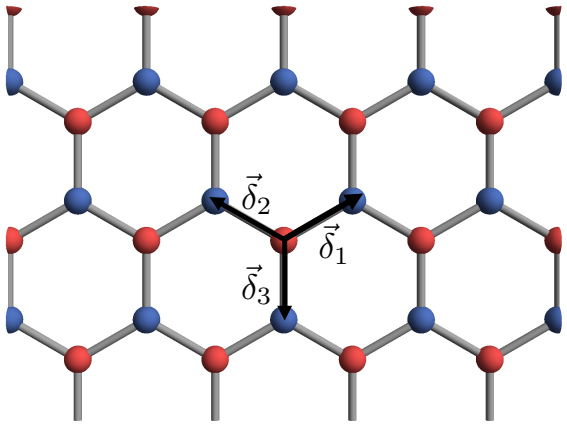


Figure 4.2: First neighbours of a honey-comb lattice. The directions of the neighbours are characterized by $\vec{\delta}_1 = a\{1/2\sqrt{3}, 1/2, 0\}$, $\vec{\delta}_2 = a\{-1/2\sqrt{3}, 1/2, 0\}$, and $\vec{\delta}_3 = a\{0, -1, 0\}$, where $a$ is the interatomic distance. These vectors are used in the tight binding expansion of the Hamiltonian.

This is the same model that is proposed for Boron-Nitride for each spin species, but with the opposite role for each sub lattice.

Following the symmetry analysis of graphene lattice we can conclude that all components of the piezospintronic tensor are zero except for

$$\lambda_{z;y,yy} = -\lambda_{z;y,xx} = \lambda_{z;x,yx}.$$

Then, our task is reduced to the evaluation of $\lambda_{z;y,yy}$. We evaluate the net spin dipolar moment created by a deformation of the lattice along the $y$ direction. The deformation of the lattice leads to a change in the hopping amplitudes. This change, by a simple geometrical analysis, is

$$\mathrm{d}t_1 = \mathrm{d}t_2 = \frac{1}{2}\mathrm{d}t_3 = \left(\frac{\partial t}{\partial a}\right)\mathrm{d}u_{yy},$$

where $t$ is the hopping amplitude at an interatomic distance $a$. The net spin dipolar moment is given by Eq. (4.5),

$$\mathrm{d}\mathbf{P}^{S}_{z,y} = \mathbf{A}^{t_1}_{z,y}\mathrm{d}t_1 + \mathbf{A}^{t_2}_{z,y}\mathrm{d}t_2 + \mathbf{A}^{t_3}_{z,y}\mathrm{d}t_3, \tag{4.11}$$

where $\mathbf{A}^{t_\mu}_{y,z}$ is defined by the relation

$$\mathbf{A}^{t_\mu}_{y,z} = \frac{\partial \mathbf{P}^S_{z,y}}{\partial t_\mu}$$

and it can be evaluated in term of spin Berry phases (Eq. (4.6)) as

$$\mathbf{A}^{t_\mu}_{\mathrm{i},j} = -\sum_\nu \int_{BZ} \frac{\mathrm{d}^2k}{(2\pi)^2} n_\nu(k) \mathrm{Im} \left\langle \frac{\partial \phi_\nu}{\partial k_j} \middle| \sigma_\mathrm{i} \middle| \frac{\partial \phi_\nu}{\partial t_\mu} \right\rangle . \tag{4.12}$$

The symmetry of the honey-comb lattice establishes a relation among the different components of $\mathbf{A}$,

$$\mathbf{A}^{t_1}_{z,y} = \mathbf{A}^{t_2}_{z,y} = -\frac{1}{2}\mathbf{A}^{t_3}_{z,y}. \tag{4.13}$$

With all symmetry relations in consideration, the final expression of the piezospintronic tensor is:

$$\lambda_{z;y,yy} = -\frac{1}{2}\left(\frac{\partial t}{\partial a}\right)\mathbf{A}^{t_3}_{z,y}. \tag{4.14}$$

The eigenstates of this Hamiltonian might be written in the coherent state basis

$$\vec{\Omega} = \left( \sum_\mathrm{i} t_\mathrm{i} \cos(\mathbf{k}\cdot\vec{\delta}_\mathrm{i}), \sum_\mathrm{i} t_\mathrm{i} \sin(\mathbf{k}\cdot\vec{\delta}_\mathrm{i}), \Delta \right); \tag{4.15}$$

$$\hat{\Omega} = \frac{\vec{\Omega}}{|\vec{\Omega}|} = (\sin\theta\cos\phi, \sin\theta\sin\phi, \cos\theta); \tag{4.16}$$

$$|\Omega\rangle = \begin{pmatrix} \mathrm{e}^{\mathrm{i}\phi}\cos\theta/2 \\ \sin\theta/2 \end{pmatrix}. \tag{4.17}$$

Then, with the following transformation The integrand in the expression for $\mathbf{A}^{t_3}_{z,y}$ might be written in terms of the Berry curvature:

$$\mathcal{F} = \nabla_Q \times \mathcal{A} = \mathrm{Im}\,\langle \nabla_Q \Omega| \times |\nabla_Q \Omega\rangle; \qquad Q = \{t, k_j\}, \tag{4.18}$$

then

$$\mathbf{A}^t_{z,j} = \int_{\mathrm{BZ}} \frac{1}{(2\pi)^2}\mathcal{F}. \tag{4.19}$$

As

$$|\mathrm{d}\Omega\rangle = \frac{1}{2}\begin{pmatrix} \mathrm{e}^{\mathrm{i}\phi}\sin\theta/2 \\ -\cos\theta/2 \end{pmatrix}\mathrm{d}\theta + \mathrm{i}\begin{pmatrix} \mathrm{e}^{\mathrm{i}\phi}\cos\theta/2 \\ 0 \end{pmatrix}\mathrm{d}\phi, \tag{4.20}$$

a straightforward calculation lead us from Eq.4.19 to

$$\mathbf{A}^{t_3}_{z,y} = \int_{BZ} \frac{\mathrm{d}^2k}{(2\pi)^2}\frac{\sin\theta}{4}\left(\frac{\partial\theta}{\partial t_3}\frac{\partial\phi}{\partial k_y} - \frac{\partial\theta}{\partial k_y}\frac{\partial\phi}{\partial t_3}\right). \tag{4.21}$$

The integral is complicated and it must be calculated numerically and his result is shown in Fig. 4.4

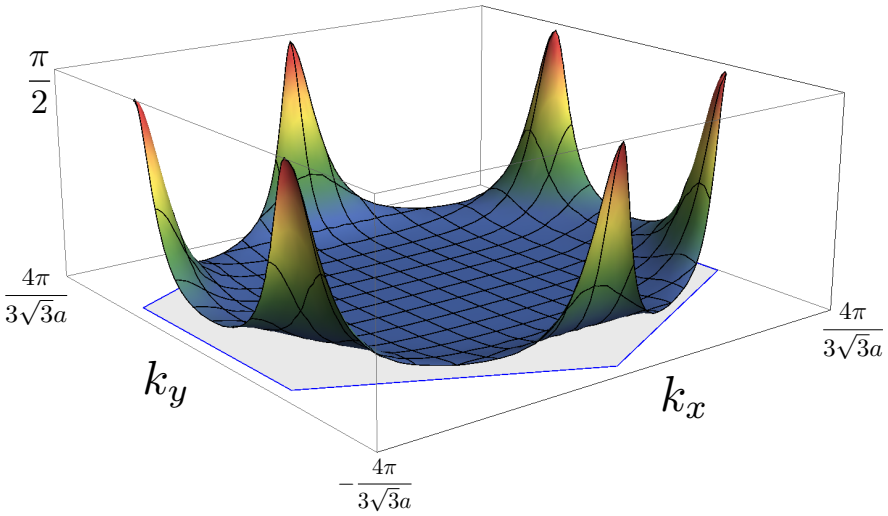


Figure 4.3: Berry curvature along the first Brillouin zone. This is the integrand of Eq. 4.21. The integral of this function will lead to the piezospintronic response of an antiferromagnetic graphene layer.

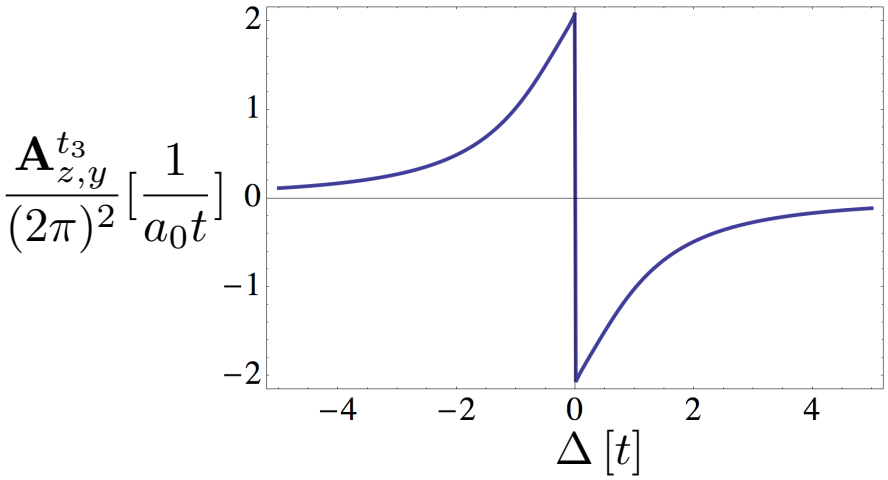


Figure 4.4: Result of the numerical integration of $\mathbf{A}^{t_3}_{z,y}$ for antiferromagnetic graphene as function of local energy $\Delta$. This result and the symmetry relations given for $\mathbf{A}$ in Eq. (4.13) the whole piezospintronic response is described.

## 4.5 Dirac graphene

One interesting result which arises from the previous section is the piezospintronic response of antiferromagnetic graphene in the long wavelength regime, known as Dirac graphene. We again make use of the coherent state representation $|\Omega\rangle$ (see Eqs. 4.15) but now we perform a series expansion around one of the edges of the Brillouin zone (see 4.4). Let us consider the point $K_+ = \{4\pi/3\sqrt{3}a_0, 0\}$. Expanding the coherent states around this point we obtain

$$\vec{\Omega}_{K_+} = \{-\frac{3}{2}a_0 t k_x, -\frac{3}{2}a_0 t k_y, \Delta\}.$$

The piezospintronic response will be again,

$$\mathbf{A}_{z,y}^{t_3} = 2\int_{BZ} \frac{\mathrm{d}^2k}{(2\pi)^2}\frac{\sin\theta}{4}\left(\frac{\partial\theta}{\partial t_3}\frac{\partial\phi}{\partial k_y} - \frac{\partial\theta}{\partial k_y}\frac{\partial\phi}{\partial t_3}\right), \tag{4.22}$$

where the factor 2 comes from the two equivalent valleys in which the expansion is performed. In this case

$$\frac{\partial\theta}{\partial t_3} = \frac{4\Delta(a_0k_y - k_x)}{|k|(9a_0^2k^2t^2 + 4\Delta^2)}; \tag{4.23}$$

$$\frac{\partial\theta}{\partial k_y} = \frac{6a_0k_y}{|k|(9a_0^2k^2t^2 + 4\Delta^2)}; \tag{4.24}$$

$$\frac{\partial\phi}{\partial t_3} = \frac{2}{3a_0tk^2}(k_y + 2a_0k_xk_y); \tag{4.25}$$

$$\frac{\partial\phi}{\partial k_y} = \frac{k_x}{k^2}, \tag{4.26}$$

from where arises

$$\mathbf{A}_{z,y}^{t_3} = -2\int_{BZ} \frac{\mathrm{d}^2k}{(2\pi)^2}\frac{3a_0t\Delta}{(9a_0^2k^2t^2 + 4\Delta^2)^{3/2}} = -\frac{1}{(2\pi)^2}\frac{2\pi\Delta}{3a_0t|\Delta|}, \tag{4.27}$$

so the piezospintronic response in the long wavelength limit just depends on the sign of $\Delta$. This solution is compared with the numerical calculation of the previous section and is shown in Fig. 4.5.

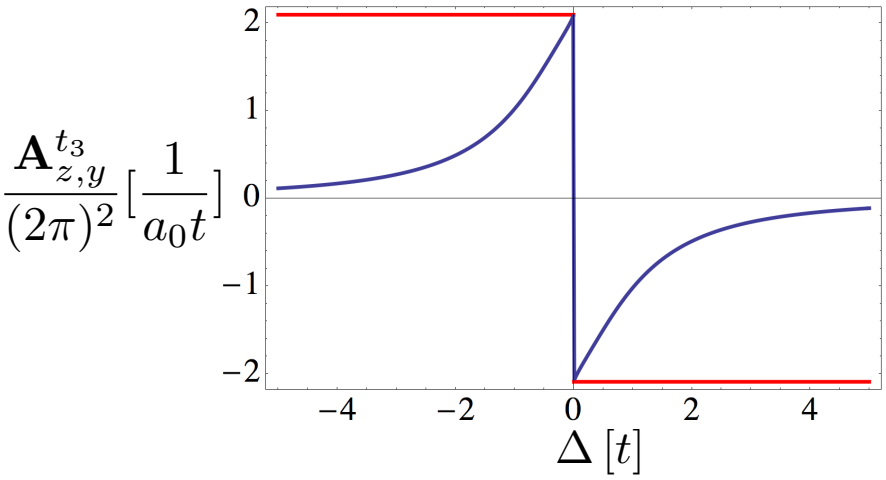


Figure 4.5: Result of the direct integration of $\mathbf{A}_{z,y}^{t_3}$ for in the long wavelength limit as function of local energy $\Delta$(red curve). The blue curve is the numerical solution shown in Fig. 4.4. The maximum(minimum) values of the curves are equal to $2\pi/3$ $(-2\pi/3)$ as we expect from Eq. 4.27.

## 4.6 Piezospintronic response of anitiferromagnetic zinc-blende

Now we discuss the piezospintronic response of antiferromagnetic zinc-blende. With the calculations of the previous sections, the extension to 3D is straightforward. As it is possible

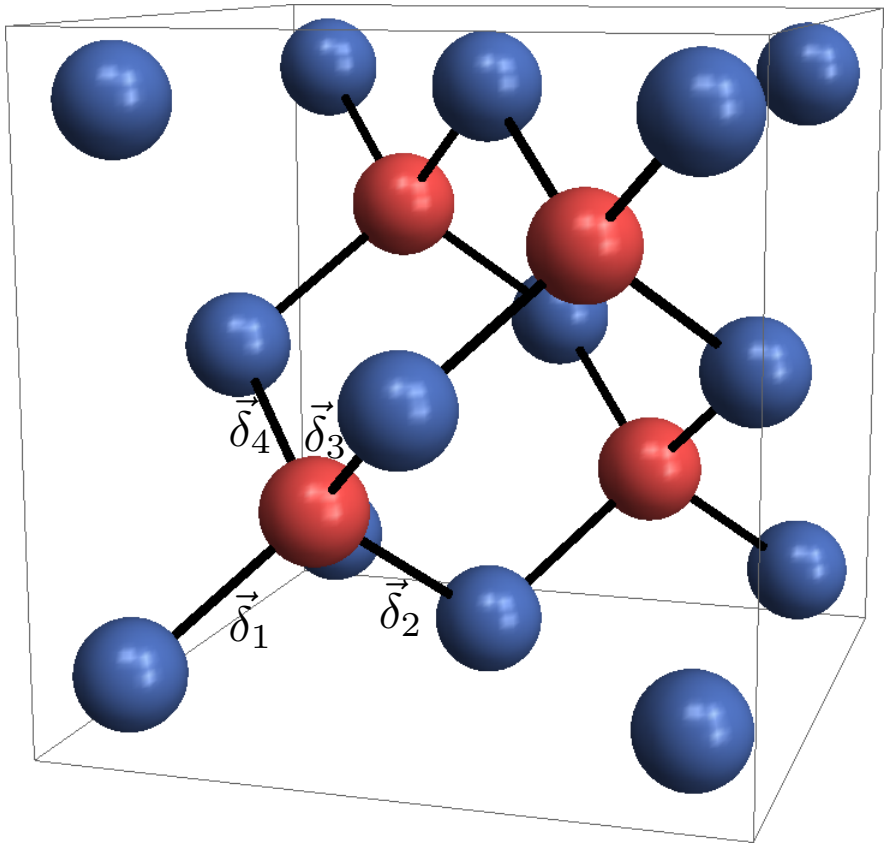


Figure 4.6: Antiferromagnetic zinc-blende unit cell. Red(blue) spheres can be thought as spin up(down) particles. As this structure has time reversal symmetry $\mathcal{I}$ and inversion symmetry $\mathcal{R}$ broken, but is invariant under $\mathcal{TI}$, we expect the system to develop a pure spin current under a strain as the piezoelectric effect is not suitable due to symmetry properties. The vectors pointing to the first neighbours, used in the tight binding expansion are defined as $\vec{\delta}_1 = -a\{1/4, 1/4, 1/4\}$, $\vec{\delta}_2 = a\{1/4, 1/4, -1/4\}$, $\vec{\delta}_3 = a\{-1/4, 1/4, 1/4\}$, and $\vec{\delta}_4 = a\{1/4, -1/4, 1/4\}$.

to see in Fig. 4.6, antiferromagnetic zinc-blende follows the same time reversal and inversion properties as antiferromagnetic graphene. Then we expect the system to develop pure spin currents by the piezospintronic effect due to the absence of piezoelectric effect. To calculate the piezospintronic response we make use again of the coherent state representation following Eqs.4.15 where the nearest neighbours vectors are defined in Fig. 4.6 and each one has a hopping amplitude $t_{\text{i}}$. The symmetry of the lattice lead us to the following expressions for

the different components of $\mathbf{A}$:

$$\begin{aligned}\mathbf{A}_z^t &\equiv \mathbf{A}_{z,x}^{t_1} = \mathbf{A}_{z,y}^{t_1} = \mathbf{A}_{z,z}^{t_1} \\ &= -\mathbf{A}_{z,x}^{t_2} = -\mathbf{A}_{z,y}^{t_2} = \mathbf{A}_{z,z}^{t_2} \\ &= \mathbf{A}_{z,x}^{t_3} = -\mathbf{A}_{z,y}^{t_3} = -\mathbf{A}_{z,z}^{t_3} \\ &= -\mathbf{A}_{z,x}^{t_4} = \mathbf{A}_{z,y}^{t_4} = -\mathbf{A}_{z,z}^{t_4}.\end{aligned} \tag{4.28}$$

Then the whole piezospintronic tensor is determined by calculating just one of the components of the above equation. In particular we can calculate

$$\mathbf{A}_{z,z}^{t_1} = \int_{BZ} \frac{\mathrm{d}^3k}{(2\pi)^3} \frac{\sin\theta}{4} \left( \frac{\partial\theta}{\partial t_1}\frac{\partial\phi}{\partial k_z} - \frac{\partial\theta}{\partial k_z}\frac{\partial\phi}{\partial t_1} \right), \tag{4.29}$$

where the Berry curvature $\mathcal{F}$ in this case is

$$\mathcal{F} = -\frac{1}{(2\pi)^3} \frac{t\Delta\left(\cos\left(\frac{k_x+k_y}{2}\right) - \cos\left(\frac{k_x+k_z}{2}\right) - \cos\left(\frac{k_y+k_z}{2}\right) + 1\right)}{16\left(\Delta^2 + 4t^2\cos\left(\frac{k_x}{2}\right)\cos\left(\frac{k_y}{2}\right) + 4t^2\cos\left(\frac{k_x}{2}\right)\cos\left(\frac{k_z}{2}\right) + 4t^2\cos\left(\frac{k_y}{2}\right)\cos\left(\frac{k_z}{2}\right) + 4t^2\right)^{3/2}}. \tag{4.30}$$

This integral is complicated an it has to be calculated numerically. The result of the numerical integral is shown in Fig.4.6

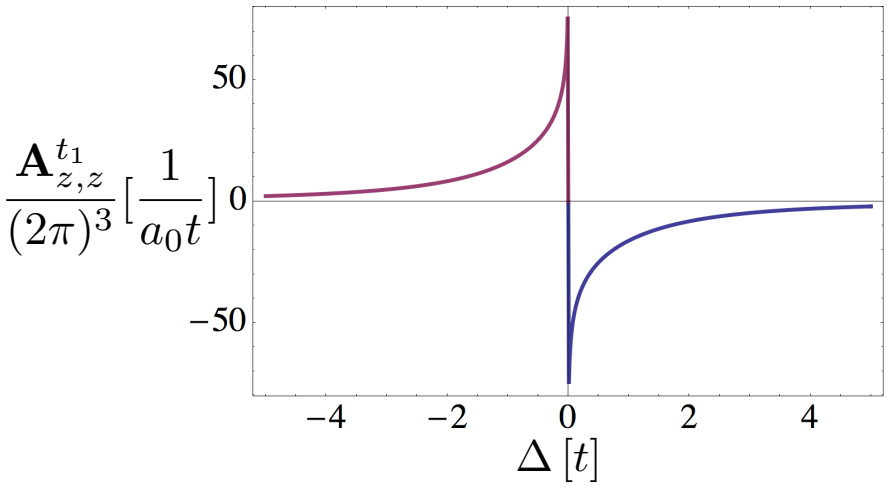


Figure 4.7: Result of the numerical integration of $\mathbf{A}_{z,z}^{t_1}$ for antiferromagnetic zinc-blende as function of local energy $\Delta$. With this result and the symmetry relations given in Eq. 4.28 the whole piezospintronic response is characterized.

## 4.7 Conclusions

Along this chapter we have introduced the piezospintronic effect and discussed the main frame in which it is involved. We have calculated the piezospintronic response of two models

whose, by symmetry principles, should have no piezoelectric response and then will develop pure spin currents under a strain. We have calculated the piezospintronic response of antiferromagnetic graphene and antiferromagnetic zinc-blende numerically. Also we have performed an analytic calculation of the piezospintronic response of antiferromagnetic graphene in the long wavelength regime obtaining concordant results with the numerical solutions.

# General conclusions

Control of antiferromagnetism has been one of the main goals to achieve and has raised a great attention in the last decades, either from a theoretical and experimental point of view. Thanks to their particular ordering, antiferromagnetic materials could be particularly useful for devices which are sensible under magnetic fields. Also, materials with this kind of ordering could be used into a novel way to store and transmit information without being affected by external magnetic fields, so preventing data losses. Another advantage of this kind of materials for this purpose is the lack of Joule heating associated with the transport of spin waves, and the absence of dipolar interactions among different domains. For these and quite more reasons the antiferromagnetism is a promising area in condensed matter physics.

In this thesis we have studied antiferromagnetism in three different contexts. First in an antiferromagnet with a non collinear ordering. We have developed an effective theory by making use of an order parameter which belongs to the rotation group. We have based our model in the exchange bias material $Mn_3Ir$. As a particular result we found that the low energy excitations behaves as sine-Gordon solitons, which opens up the control of this wide family of topological soliton in this kind of systems. This work needs to be continued by analyzing the effects of Dzyaloshinskii-Moriya interaction (DMI), and of course we need to expand our model to understand the behavior of the system under the effect of electrical or spin currents.

We have analyzed antiferromagnetic heterostructures with a modulated anisotropy or magnetic field and opened the field of antiferromagnetic magnonic crystals. As main result we have characterized the spin wave spectra of this systems and found that under the named modulations it is possible to constraint the spectrum into a band-like structure. This spectrum also shows the properties of the chirality of the elemental excitations of the system. This work could be expanded by including another kind of interactions, as DMI for example.

Finally we have studied the quantum effects on a spin system under strain and the spin currents which this generates by the piezospintronic effect. We have focused our analysis in two hypothetical models: antiferromagnetic graphene, and antiferromagnetic zinc-blende. By making use of the theory proposed in [16] we have characterized the piezospintronic response of the named models. This work could lead to control the generation and detection of pure spin currents altogether with other phenomena as the inverse spin Hall effect for example. For that could be suitable to understand the injection of this kind of currents between our models and a ferromagnetic insulator.

# Bibliography


[1] A. H. Macdonald and M Tsoi. Antiferromagnetic metal spintronics. *Philosophical transactions. Series A, Mathematical, physical, and engineering sciences*, 369(1948):3098–3114, 2011.

[2] Rembert Duine. Spintronics: An alternating alternative. *Nat Mater*, 10(5):344–345, may 2011.

[3] Fabio Pulizzi. Spintronics. *Nat Mater*, 11(5):367, may 2012.

[4] Jairo Sinova and Igor Žutić. New moves of the spintronics tango. *Nature Materials*, 11(5):368–371, 2012.

[5] Louis Néel. Magnetism and the local molecular field. *Science*, 174(4013):985–992, 1971.

[6] T Jungwirth, X Marti, P Wadley, and J Wunderlich. Antiferromagnetic spintronics. *Nat Nano*, 11(3):231–241, mar 2016.

[7] George E Uhlenbeck and Samuel Goudsmit. Spinning electrons and the structure of spectra. *Nature*, 117:264–265, 1926.

[8] W Pauli Jr. Über gasentartung und paramagnetismus. *Zeitschrift für Physik*, 41(2):81–102, 1927.

[9] Paul AM Dirac. The quantum theory of the electron. In *Proceedings of the Royal Society of London A: Mathematical, Physical and Engineering Sciences*, volume 117, pages 610–624. The Royal Society, 1928.

[10] Werner Heisenberg. Mehrkörperproblem und resonanz in der quantenmechanik. In *Original Scientific Papers Wissenschaftliche Originalarbeiten*, pages 456–471. Springer, 1985.

[11] Paul AM Dirac. On the theory of quantum mechanics. In *Proceedings of the Royal Society of London A: Mathematical, Physical and Engineering Sciences*, volume 112, pages 661–677. The Royal Society, 1926.

[12] FDM Haldane. Nonlinear field theory of large-spin heisenberg antiferromagnets: semiclassically quantized solitons of the one-dimensional easy-axis néel state. *Physical Review Letters*, 50(15):1153, 1983.

[13] A S Nunez, R A Duine, Paul Haney, and A H MacDonald. Theory of spin torques and giant magnetoresistance in antiferromagnetic metals. *Physical Review B*, 73(21), jun 2006.

[14] P M Haney, D Waldron, R A Duine, A S Nunez, H Guo, and A H MacDonald. Ab initio giant magnetoresistance and current-induced torques in Cr/Au/Cr multilayers. *Physical Review B*, 75(17), may 2007.

[15] E. V. Gomonay and V. M. Loktev. Spintronics of antiferromagnetic systems. *Low Temperature Physics*, 40(1):17–35, jan 2014.

[16] Alvaro S Nunez. Theory of the piezo-spintronic effect. *Solid State Communications*, 198(SI):18–21, nov 2014.

[17] R.E. Troncoso, C. Ulloa, F. Pesce, and A.S. Nunez. Antiferromagnetic magnonic crystals. *Physical Review B - Condensed Matter and Materials Physics*, 92(22), 2015.

[18] Sergei Urazhdin and Nicholas Anthony. Effect of polarized current on the magnetic state of an antiferromagnet. *Physical Review Letters*, 99(4), jul 2007.

[19] Z Wei, A Sharma, A S Nunez, P M Haney, R A Duine, J Bass, A H MacDonald, and M Tsoi. Changing exchange bias in spin valves with an electric current. *Physical Review Letters*, 98(11), mar 2007.

[20] Paul M Haney and A H MacDonald. Current-induced torques due to compensated antiferromagnets. *Physical Review Letters*, 100(19), may 2008.

[21] Yuan Xu, Shuai Wang, and Ke Xia. Spin-transfer torques in antiferromagnetic metals from first principles. *Physical Review Letters*, 100(22), jun 2008.

[22] Helen V. Gomonay and Vadim M. Loktev. Spin transfer and current-induced switching in antiferromagnets. *Physical Review B*, 81(14), apr 2010.

[23] E V Gomonay and V. A. Lvov. Phenomenological study of phase-transition in non-collinear antiferromagnets of metallic perovskite type. *Phase Transitions*, 38(1, A):15–31, 1992.

[24] J M Logan, H C Kim, D Rosenmann, Z Cai, R Divan, O G Shpyrko, and E D Isaacs. Antiferromagnetic domain wall engineering in chromium films. *Applied Physics Letters*, 100(19), may 2012.

[25] B A Ivanov and A K Kolezhuk. Solitons in low-dimensional antiferromagnets. *Fizika Nizkikh Temperatur*, 21:355–389, 1995.

[26] Kjetil M D Hals, Yaroslav Tserkovnyak, and Arne Brataas. Phenomenology of Current-Induced Dynamics in Antiferromagnets. *Physical Review Letters*, 106(10), mar 2011.

[27] A C Swaving and R A Duine. Current-induced torques in continuous antiferromagnetic textures. *Physical review B*, 83(5), feb 2011.

[28] Ran Cheng and Qian Niu. Electron dynamics in slowly varying antiferromagnetic texture. *Physical Review B*, 86(24), dec 2012.

[29] Erlend G Tveten, Tristan Mueller, Jacob Linder, and Arne Brataas. Intrinsic magnetization of antiferromagnetic textures. *Physical Review B*, 93(10), mar 2016.

[30] Erlend G Tveten, Alireza Qaiumzadeh, O A Tretiakov, and Arne Brataas. Staggered Dynamics in Antiferromagnets by Collective Coordinates. *Physical Review Letters*, 110(12), mar 2013.

[31] Junya Shibata, Gen Tatara, and Hiroshi Kohno. A brief review of field- and current-driven domain-wall motion. *Journal of Physics D: Applied Physics*, 44(38):384004, 2011.

[32] Stuart S P Parkin, Masamitsu Hayashi, and Luc Thomas. Magnetic domain-wall racetrack memory. *Science*, 320(5873):190–194, apr 2008.

[33] K A Omari and T J Hayward. Chirality-Based Vortex Domain-Wall Logic Gates. *Physical Review Applied*, 2(4), oct 2014.

[34] A Chubukov. Order from disorder in a kagome antiferromagnet. *Physical Review Letters*, 69(5):832–835, aug 1992.

[35] D A Huse and A D Rutenberg. Classical antiferromagnets on the kagome lattice. *Physical Review B*, 45(13):7536–7539, apr 1992.

[36] S Sachdev. Kagome-lattice and triangular-lattice Heisenberg antiferromagnets - ordering from quantum fluctuations and quantum disordered ground-states with unconfined bosonic spinons. *Physical Review B*, 45(21):12377–12396, jun 1992.

[37] I Ritchey, P Chandra, and P Coleman. Spin folding in the 2-dimensional Heisenberg kagome antiferromagnet. *Physical Review B*, 47(22):15342–15345, jun 1993.

[38] A Kohn, A Kovács, R Fan, G J McIntyre, R C C Ward, and J P Goff. The antiferromagnetic structures of IrMn3 and their influence on exchange-bias. *Scientific reports*, 3:2412, 2013.

[39] I Tomeno, H N Fuke, H Iwasaki, M Sahashi, and Y Tsunoda. Magnetic neutron scattering study of ordered Mn3Ir. *Journal of Applied Physics*, 86(7):3853–3856, oct 1999.

[40] M. D. Leblanc, M. L. Plumer, J. P. Whitehead, and B. W. Southern. Monte Carlo simulations of the fcc kagome lattice: Competition between triangular frustration and cubic anisotropy. *Physical Review B - Condensed Matter and Materials Physics*, 88(9):1–6, 2013.

[41] L. Szunyogh, B. Lazarovits, L. Udvardi, J. Jackson, and U. Nowak. Giant magnetic anisotropy of the bulk antiferromagnets IrMn and IrMn 3 from first principles. *Physical Review B*, 79(2):1–4, 2009.

[42] V Hemmati, M L Plumer, J P Whitehead, and B W Southern. Monte Carlo simulations

of magnetic ordering in the fcc kagome lattice. *Physical Review B*, 86(10), sep 2012.

[43] Hua Chen, Qian Niu, and A. H. Macdonald. Anomalous hall effect arising from noncollinear antiferromagnetism. *Physical Review Letters*, 112(1):1–5, 2014.

[44] T. Dombre and N. Read. Nonlinear models for triangular quantum antiferromagnets. *Physical Review B*, 39(10):6797–6801, 1989.

[45] Aleksandr F Andreev and Vladimir I Marchenko. Symmetry and the macroscopic dynamics of magnetic materials. *Soviet Physics Uspekhi*, 23(1):21, 1980.

[46] A B Harris, C Kallin, and A J Berlinsky. Possible Neel orderings of the kagome antiferromagnet. *Physical Review B*, 45(6):2899–2919, feb 1992.

[47] M. D. LeBlanc, B. W. Southern, M. L. Plumer, and J. P. Whitehead. Spin waves in the anisotropic fcc kagome antiferromagnet. *Physical Review B*, 90(14):1–7, 2014.

[48] E. V. Gomonaj and V. A. Lvov. Phenomenological consideration of spin-wave spectrum in noncollinear antiferromagnet Mn3NiN. *Journal of Magnetism and Magnetic Materials*, 86(2-3):301–306, may 1990.

[49] R. Rajaraman. Solitons and instantons. *North-Holland*, 1982.

[50] Jesús Cuevas-Maraver, Panayotis G Kevrekidis, and Floyd Williams. The sine-gordon model and its applications.

[51] N. D. Mermin. Topological theory of defects in ordered media. *Reviews of Modern Physics*, 51(3):591–648, 1979.

[52] Mikio Nakahara. *Geometry, topology and physics*. CRC Press, 2003.

[53] Yi Zhang, Ying Ran, and Ashvin Vishwanath. Topological insulators in three dimensions from spontaneous symmetry breaking. *Physical Review B*, 79(24), jun 2009.

[54] Sam Treiman and Roman Jackiw. *Current algebra and anomalies*. Princeton University Press, 2014.

[55] Aleksandr Michajlovič Polyakov and AM Poljakov. *Gauge fields and strings*, volume 140. Harwood academic publishers Chur, 1987.

[56] Olena Gomonay. Berry-phase effects and electronic dynamics in a noncollinear antiferromagnetic texture. *Physical Review B*, 91(14):1–11, 2015.

[57] R Shankar. More SO(3) monopoles. *Physical Review D*, 14(4):1107–1116, 1976.

[58] D. Grundler. Reconfigurable magnonics heats up. *Nature Physics*, 11(6):438–441, 2015.

[59] A. V. Chumak, V. I. I. Vasyuchka, A. A. A. Serga, and B. Hillebrands. Magnon spintronics. *Nature Physics*, 11(6):453–461, 2015.

[60] V. V. Kruglyak, S. O. Demokritov, and D. Grundler. Magnonics. *Journal of Physics D: Applied Physics*, 43(26):264001, 2010.

[61] A V Chumak, V S Tiberkevich, A D Karenowska, A. A. A. Serga, J F Gregg, A N Slavin, and B Hillebrands. All-linear time reversal by a dynamic artificial crystal. *Nature communications*, 1(Dmc):141, 2010.

[62] M. Krawczyk and D. Grundler. Review and prospects of magnonic crystals and devices with reprogrammable band structure. *Journal of physics. Condensed matter : an Institute of Physics journal*, 26(12):123202, 2014.

[63] Fusheng Ma, Yan Zhou, H. B. Braun, and W. S. Lew. Skyrmion-Based Dynamic Magnonic Crystal. *Nano Letters*, 15(6):4029–4036, 2015.

[64] M Mruczkiewicz, P Gruszecki, M Zelent, and M Krawczyk. Collective dynamical skyrmions excitations in magnonic crystal. *arXiv preprint arXiv:1502.08024*, 2015.

[65] RA Gallardo, A Banholzer, K Wagner, M Körner, K Lenz, M Farle, J Lindner, J Fassbender, and P Landeros. Splitting of spin-wave modes in thin films with arrays of periodic perturbations: theory and experiment. *New Journal of Physics*, 16(2):023015, 2014.

[66] Helen V. Gomonay, Roman V. Kunitsyn, and Vadim M. Loktev. Symmetry and the macroscopic dynamics of antiferromagnetic materials in the presence of spin-polarized current. *Physical Review B*, 85(13), apr 2012.

[67] Joseph Barker and Oleg A Tretiakov. Static and dynamical properties of antiferromagnetic skyrmions in the presence of applied current and temperature. *Physical review letters*, 116(14):147203, 2016.

[68] Xichao Zhang, Yan Zhou, and Motohiko Ezawa. Antiferromagnetic skyrmion: Stability, creation and manipulation. *Scientific Reports*, 6:24795 EP –, 04 2016.

[69] Manfred Fiebig, Nguyen Phuc Duong, Takuya Satoh, Bas B Van Aken, Kenjiro Miyano, Yasuhide Tomioka, and Yoshinori Tokura. Ultrafast magnetization dynamics of antiferromagnetic compounds. *Journal of Physics D: Applied Physics*, 41(16):164005, 2008.

[70] F Máca, J Mašek, O Stelmakhovych, X Martí, H Reichlová, K Uhlířová, P Beran, P Wadley, V Novák, and T Jungwirth. Room-temperature antiferromagnetism in cumnas. *Journal of Magnetism and Magnetic Materials*, 324(8):1606–1612, 2012.

[71] NB Weber, H Ohldag, H Gomonaj, and FU Hillebrecht. Magnetostrictive domain walls in antiferromagnetic nio. *Physical review letters*, 91(23):237205, 2003.

[72] JP Kotthaus and V Jaccarino. Antiferromagnetic-resonance linewidths in mn f 2. *Physical Review Letters*, 28(25):1649, 1972.

[73] Fred M Johnson and Arthur H Nethercot Jr. Antiferromagnetic resonance in mn f 2. *Physical Review*, 114(3):705, 1959.

[74] RC Ohlmann and M Tinkham. Antiferromagnetic resonance in fe f 2 at far-infrared frequencies. *Physical Review*, 123(2):425, 1961.

[75] J Strempfer, U Rütt, and W Jauch. Absolute spin magnetic moment of fef 2 from high energy photon diffraction. *Physical review letters*, 86(14):3152, 2001.

[76] Philip W Anderson. An approximate quantum theory of the antiferromagnetic ground state. *Physical Review*, 86(5):694, 1952.

[77] Co G Shull, WA Strauser, and EO Wollan. Neutron diffraction by paramagnetic and antiferromagnetic substances. *Physical Review*, 83(2):333, 1951.

[78] Assa Auerbach. *Interacting electrons and quantum magnetism*. Springer Science & Business Media, 2012.

[79] LP Pitaevskii and EM Lifshitz. Statistical physics part ii, volume 9 of course of theoretical physics, 1980.

[80] VS L'vov and MI Shirokov. Nonlinear theory of parametric excitation of spin waves in antiferromagnets. *Zh. Eksp. Teor. Fiz*, 67:1932–1948, 1974.

[81] Victor S L'vov. *Wave turbulence under parametric excitation: applications to magnets*. Springer Science & Business Media, 2012.

[82] John MD Coey. *Magnetism and magnetic materials*. Cambridge University Press, 2010.

[83] Charles Kittel. *Introduction to solid state physics*. Wiley, 2005.

[84] AV Chumak, T Neumann, AA Serga, B Hillebrands, and MP Kostylev. A current-controlled, dynamic magnonic crystal. *Journal of Physics D: Applied Physics*, 42(20):205005, 2009.

[85] Junren Shi, Ping Zhang, Di Xiao, and Qian Niu. Proper definition of spin current in spin-orbit coupled systems. *Physical review letters*, 96(7):076604, 2006.

[86] Lev D Landau and EM Lifshitz. Theory of elasticity, vol. 7. *Course of Theoretical Physics*, 3:109, 1986.

[87] Lars Onsager. Reciprocal relations in irreversible processes. i. *Physical Review*, 37(4):405, 1931.

[88] Richard M Martin. Comment on calculations of electric polarization in crystals. *Physical Review B*, 9(4):1998, 1974.

[89] Raffaele Resta. Theory of the electric polarization in crystals. *Ferroelectrics*, 136(1):51–55, 1992.

[90] RD King-Smith and David Vanderbilt. Theory of polarization of crystalline solids. *Physical Review B*, 47(3):1651, 1993.

[91] Gerardo Ortiz and Richard M Martin. Macroscopic polarization as a geometric quantum phase: Many-body formulation. *Physical Review B*, 49(20):14202, 1994.

[92] Raffaele Resta. Macroscopic polarization in crystalline dielectrics: the geometric phase approach. *Reviews of modern physics*, 66(3):899, 1994.

[93] Shigeki Onoda, Shuichi Murakami, and Naoto Nagaosa. Topological nature of polarization and charge pumping in ferroelectrics. *Physical review letters*, 93(16):167602, 2004.

[94] Junichi Iwasaki, Masahito Mochizuki, and Naoto Nagaosa. Current-induced skyrmion dynamics in constricted geometries. *Nature nanotechnology*, 8(10):742–747, 2013.

# Appendix A

# Spin path integral and Berry phase

In this appendix we derive from first principles an expression for the Euclidean action (i.e in imaginary time) for the dynamics of a spin evolving by an arbitrary Hamiltonian $H[\mathbf{\Omega}]$ by the path integral formalism. Here emerges in a completely natural way the Berry phase associated with the quantum effects. We also find a gauge independent expression for the Berry phase.

## A.1 Euclidean action from path integral

We start from the fact that a partition function can be written as a path integral in imaginary time. The partition function in the canonical ensemble is defined as

$$Z = \mathrm{Tr}\left[\mathrm{e}^{-\beta H[\hat{\mathbf{S}}]}\right], \tag{A.1}$$

where $\beta = 1/k_B T$ is the inverse thermal energy. The exponential in Eq.A.1 could be interpreted as an evolution operator in imaginary time, from $\tau = 0$ to $\tau = \hbar\beta$. We divide this imaginary time interval into infinitesimal pieces $\Delta\tau = \hbar\beta/N$ with $N$ large. Then is possible to split the exponential into a product of exponentials and expand them to first order in $\Delta\tau$

$$\begin{aligned} Z &= \mathrm{Tr}\left[\mathrm{e}^{-\sum_{j=0}^{N-1}\Delta\tau H[\hat{\mathbf{S}}]/\hbar}\right] \\ &= \mathrm{Tr}\left[\left(1-\Delta\tau H[\hat{\mathbf{S}}]\right)^{N}\right]. \end{aligned} \tag{A.2}$$

Now we need a proper set of states in order to translate the operators in last equation into numbers. We are looking for something with the following property

$$\langle\mathbf{\Omega}|\,\hat{\mathbf{S}}\,|\mathbf{\Omega}\rangle = \hbar S\hat{\mathbf{\Omega}} \tag{A.3}$$

with $\mathbf{\Omega}$ a unit vector. It is possible to achieve this by the so-called spin coherent states which are a family of spin states reached by applying the rotation operator $\mathcal{R} = \mathrm{e}^{\mathrm{i}S^z\phi}\mathrm{e}^{\mathrm{i}S^y\theta}\mathrm{e}^{\mathrm{i}S^x\chi}$ to

the maximally polarized spin state $|S,S\rangle$

$$|\mathbf{\Omega}\rangle = \mathrm{e}^{\mathrm{i}S^z\phi}\mathrm{e}^{\mathrm{i}S^y\theta}\mathrm{e}^{\mathrm{i}S^x\chi}\,|S,S\rangle\,, \tag{A.4}$$

where $\mathbf{\Omega} = (\sin\theta\,\cos\phi, \sin\theta\,\sin\phi, \cos\theta)$, parametrizes the spin coherent state. The angle $\chi$ can be chosen arbitrarily (it is a gauge freedom so it can be fixed). The two independent angles are defined such that

$$\theta \;\in\; [0,\pi], \quad \phi \;\in\; [-\pi,\pi).$$

Without any proof we show here some properties of spin coherent states $|\mathbf{\Omega}\rangle$. An explicit expression for these states is given (up to a phase factor) by

$$|\mathbf{\Omega}\rangle = \sum_{m_s=-S}^{m_s=S} \binom{2S}{S+m_s}^{1/2} \mathrm{e}^{-\mathrm{i}(m_s-S)\phi} \left(\cos\frac{\theta}{2}\right)^{S+m_s} \left(\sin\frac{\theta}{2}\right)^{S-m_s} |S,m_s\rangle\,,$$

then the overlap between two different states is given by

$$\langle\mathbf{\Omega}'\,|\mathbf{\Omega}\rangle = \left(\cos\frac{\theta}{2}\cos\frac{\theta'}{2} + \sin\frac{\theta}{2}\sin\frac{\theta'}{2}\mathrm{e}^{-\mathrm{i}(\phi-\phi')}\right)^{2S}.$$

From this last result arises that the overlap between two infinitesimally separated states is given by

$$\langle\mathbf{\Omega}'\,|\mathbf{\Omega}\rangle = 1 + \mathrm{i}S(\phi'-\phi)(\cos\theta - 1). \tag{A.5}$$

The closure relation which coherent spin states obey is

$$\mathbf{1} = \frac{2S+1}{4\pi}\int \mathrm{d}\mathbf{\Omega}\,|\mathbf{\Omega}\rangle\,\langle\mathbf{\Omega}|\,,$$

where $\int \mathrm{d}\mathbf{\Omega} = \int_{-1}^{1}\mathrm{d}(\cos\theta)\int_0^{2\pi}\mathrm{d}\phi$. In this representation the trace of an operator $\hat{\mathcal{O}}$ is

$$\mathrm{Tr}\left[\hat{\mathcal{O}}\right] = \frac{2S+1}{4\pi}\int \mathrm{d}\mathbf{\Omega}\;\langle\mathbf{\Omega}|\,\hat{\mathcal{O}}\,|\mathbf{\Omega}\rangle\,.$$

Now we are in conditions to continue the road for the spin path integral. Inserting the closure relation in between the products in Eq. (A.2)

$$\begin{aligned} Z = \left(\frac{2S+1}{4\pi}\right)^N \left(\prod_{j=1}^{N-1}\int \mathrm{d}\mathbf{\Omega}_j\right) \langle\mathbf{\Omega}_0|\left(1-\Delta\tau H[\hat{\mathbf{S}}]/\hbar\right)|\mathbf{\Omega}_{N-1}\rangle \\ \langle\mathbf{\Omega}_{N-1}|\left(1-\Delta\tau H[\hat{\mathbf{S}}]/\hbar\right)|\mathbf{\Omega}_{N-2}\rangle \ldots \langle\mathbf{\Omega}_1|\left(1-\Delta\tau H[\hat{\mathbf{S}}]/\hbar\right)|\mathbf{\Omega}_0\rangle\,. \end{aligned} \tag{A.6}$$

Using the properties of the coherent spin states

$$\begin{aligned} \langle\mathbf{\Omega}_{j+1}|\left(1-\Delta\tau H[\hat{\mathbf{S}}]/\hbar\right)|\mathbf{\Omega}_j\rangle &\approx (1-\Delta\tau H[\hbar S\mathbf{\Omega}_j]/\hbar + \mathrm{i}S(\phi_{j+1}-\phi_j)(\cos\theta_j-1)) + \mathcal{O}(\Delta\tau^2) \\ &= \mathrm{e}^{(1-\Delta\tau H[\hbar S\mathbf{\Omega}_j]/\hbar + \mathrm{i}S(\phi_{j+1}-\phi_j)(\cos\theta_j-1))}, \end{aligned} \tag{A.7}$$

so the partition function is written as

$$Z = \left(\frac{2S+1}{4\pi}\right)^N \left(\prod_{j=1}^{N-1} \int \mathrm{d}\mathbf{\Omega}_j\right) \times \exp\left\{\sum_{j=0}^{N-1} \Delta\tau \left[\mathrm{i}S\left(\frac{\phi_{j+1}-\phi_j}{\Delta\tau}\right)(\cos\theta_j - 1) - \frac{H[\hbar S\mathbf{\Omega}_j]}{\hbar}\right]\right\}, \tag{A.8}$$

were we have assumed periodic boundary conditions given by $\phi_0 = \phi_N$ and $\theta_0 = \theta_N$. Finally we take the continuum limit $N \to \infty$, $\Delta\tau \to 0$, and $N\Delta\tau = \hbar\beta$. Then we identify

$$\tau \to j\Delta\tau;$$

$$\phi_j \to \phi(\tau);$$

$$\theta_j \to \theta(\tau);$$

$$\Delta\tau \to \mathrm{d}\tau;$$

$$\frac{\phi_{j+1}-\phi_j}{\Delta\tau} \to \frac{\mathrm{d}\phi}{\mathrm{d}\tau} = \dot{\phi}(\tau);$$

$$\left(\frac{2S+1}{4\pi}\right)^N \left(\prod_{j=1}^{N-1} \int \mathrm{d}\mathbf{\Omega}_j\right) \to \mathcal{D}\mathbf{\Omega}(\tau).$$

So we find that the partition function is given as a path integral over all periodic paths $\mathbf{\Omega}(\tau)$ on the unit sphere,

$$Z = \int_{\mathbf{\Omega}(0)=\mathbf{\Omega}(\hbar\beta)} \mathcal{D}\mathbf{\Omega}(\tau) \exp\left\{-\frac{1}{\hbar}\mathcal{A}_E[\mathbf{\Omega}]\right\}. \tag{A.9}$$

In the last expression the Euclidean action is given by the functional

$$\mathcal{A}_E[\mathbf{\Omega}] = \int_0^{\hbar\beta} \mathrm{d}\tau \left\{\mathrm{i}\hbar S\dot{\phi}(\tau)[1-\cos\theta(\tau)] + H[\hbar S\mathbf{\Omega}(\tau)]\right\}. \tag{A.10}$$

## A.2 Berry phase

If we keep an eye on the Euclidean action we notice that the usual term involving the Hamiltonian is present, but also there is a phase factor given by

$$\exp\left(-\mathrm{i}S\int_0^{\hbar\beta} \mathrm{d}\tau\dot{\phi}(\tau)[1-\cos\theta(\tau)]\right). \tag{A.11}$$

It is direct that

$$\omega = \int_0^{\hbar\beta} \mathrm{d}\tau\dot{\phi}(\tau)[1-\cos\theta(\tau)] = \oint \mathrm{d}\phi(1-\cos\theta_\phi), \tag{A.12}$$

then the nature of this phase is completely geometric, that means, it depends only in the trajectory along the unit sphere and not on the time dependence. This functional is also known as *Berry phase*, since it describes the phase acquired by a spin in an adiabatically

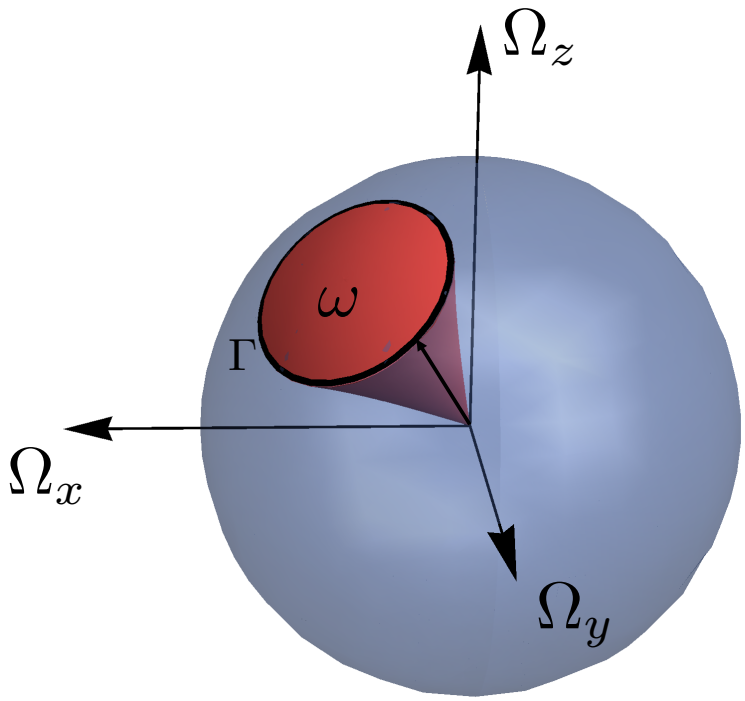


Figure A.1: Cartoon of the Berry phase $\omega$. The area enclosed by the path followed by $\mathbf{\Omega}$ in a cycle is proportional to the flux of magnetic field generated by a magnetic monopole. By Stokes theorem this area is proportional to the line integral of the vector potential $\mathbf{A}$ along the boundary $\Gamma$.

rotating magnetic field parallel to $\mathbf{\Omega}(\tau)$. The Berry phase measures the area which the path of $\mathbf{\Omega}(\tau)$ encloses on the unit sphere.

It is completely useful to express the Berry phase $\omega$ in a gauge invariant form, that is without specifying a parametrization of the sphere as we have done with the angles $\theta$ and $\phi$. Let's consider a magnetic monopole which generates a magnetic field $\mathbf{B}$, the flux of the field across a patch $S_\Gamma$ of an unit sphere will be given by

$$\omega = \int_{S_\Gamma} \mathbf{B} \cdot \mathrm{d}\mathbf{S},$$

as $\mathbf{B} = \nabla \times \mathbf{A}$, and by Stokes theorem, the flux, corresponding to the area enclosed by the path of the vector $\mathbf{\Omega}$, will follow

$$\omega = \oint_\Gamma \mathrm{d}\tau \mathbf{A}(\mathbf{\Omega}) \cdot \dot{\mathbf{\Omega}} = \oint_\Gamma \mathrm{d}\mathbf{\Omega} \cdot \mathbf{A}(\mathbf{\Omega}).$$

The vector potential of a magnetic monopole has several representations. Every function such that $\nabla_{\mathbf{\Omega}} \times \mathbf{A} = \mathbf{\Omega}$ is suitable.

# Appendix B

# Landau-Lifshitz-Gilbert equation

In this chapter we introduce the Landau-Lifshitz-Gilbert (LLG) equation, which is the newest way to model magnetization dynamics in absence of electrical or spin currents. We show two ways to solve LLG equation. The first is an extremely simple Euler integration, and the second is by making use of the rotation operators as in quantum mechanics.

## B.1 The equation

Following [94], the LLG equation in absence of external current is

$$\dot{\mathbf{S}} = -\gamma \mathbf{S} \times \mathbf{B}_{\text{eff}} + \alpha \mathbf{S} \times \dot{\mathbf{S}}, \tag{B.1}$$

where $\gamma$ is the gyromagnetic ratio. The second term denotes the Gilbert damping, where $\alpha$ is the tendency of the magnetization to stop the precession around the effective field $\mathbf{B}_{\text{eff}} = -(1/\hbar\gamma)(\partial\mathcal{H}/\partial\mathbf{S})$. Along this section we will consider that the magnitude of each local magnetic moment is $|\mathbf{S}| = 1$. Replacing the expression for $\dot{\mathbf{S}}$ in the right side of Eq.(B.1) it is straightforward that

$$\dot{\mathbf{S}} = \frac{-\gamma \mathbf{S} \times \mathbf{B}_{\text{eff}} - \alpha\gamma \mathbf{S} \times (\mathbf{S} \times \mathbf{B}_{\text{eff}})}{1 + \alpha^2}. \tag{B.2}$$

This equation can be written as

$$\dot{\mathbf{S}} = \mathbf{H} \times \mathbf{S}, \tag{B.3}$$

where

$$\mathbf{H} = \frac{\gamma}{1 + \alpha^2} \left( \mathbf{B}_{\text{eff}} + \alpha \mathbf{S} \times \mathbf{B}_{\text{eff}} \right).$$

Equation (B.3) can be easily integrated by a long list of methods. For our numerical simulations we have performed an integration by Euler's method,

$$\mathbf{S}(t + \mathrm{d}t) = \mathbf{S}(t) + \mathrm{d}t \mathbf{H} \times \mathbf{S}. \tag{B.4}$$

Of course as this method does not preserve the norm of the vector it is imperative to normalize the resulting vector in each step.

A more elegant way to solve Eq. B.3 comes from the angular momentum generators of quantum mechanics. As their components follow

$$\dot{S}_{\mathrm{i}} = \varepsilon_{\mathrm{i}jk} H_j S_k = \mathbf{L}\cdot\mathbf{H}\; S_k,$$

the solution of this equation has the form

$$\mathbf{S}(t) = \exp\left(\int_0^t \mathbf{L}\cdot\mathbf{H}\right)\mathbf{S}(0),$$

which is nothing but an evolution operator spanned by the generators

$$L_x = \begin{pmatrix} 0 & 0 & 0 \\ 0 & 0 & -1 \\ 0 & 1 & 0 \end{pmatrix}; \qquad L_y = \begin{pmatrix} 0 & 0 & 1 \\ 0 & 0 & 0 \\ -1 & 0 & 0 \end{pmatrix}; \qquad L_z = \begin{pmatrix} 0 & -1 & 0 \\ 1 & 0 & 0 \\ 0 & 0 & 0 \end{pmatrix}. \tag{B.5}$$

Assuming that $t$ is infintesimal, $t \to \mathrm{d}t$, then

$$\mathbf{S}(\mathrm{d}t) = \exp\left(\mathbf{L}\cdot\mathbf{H}\;\mathrm{d}t\right)\mathbf{S}(0) = \frac{\exp\left(\mathbf{L}\cdot\mathbf{H}\;\mathrm{d}t/2\right)}{\exp\left(-\mathbf{L}\cdot\mathbf{H}\;\mathrm{d}t/2\right)}\mathbf{S}(0) \approx \frac{\mathbb{I}+\mathbf{L}\cdot\mathbf{H}\;\mathrm{d}t/2}{\mathbb{I}-\mathbf{L}\cdot\mathbf{H}\;\mathrm{d}t/2}\mathbf{S}(0)$$

$$\Rightarrow \left[\mathbb{I}-\mathbf{L}\cdot\mathbf{H}\;\frac{\mathrm{d}t}{2}\right]\mathbf{S}(\mathrm{d}t) = \left[\mathbb{I}+\mathbf{L}\cdot\mathbf{H}\;\frac{\mathrm{d}t}{2}\right]\mathbf{S}(0). \tag{B.6}$$

Equation $B.6$ is analogous to the linear algebra problem $A\mathbf{x} = \mathbf{b}$, where we identify $A = [\mathbb{I} - \mathbf{L}\cdot\mathbf{H}\;\mathrm{d}t/2]$, and $\mathbf{b} = [\mathbb{I} + \mathbf{L}\cdot\mathbf{H}\;\mathrm{d}t/2]\,\mathbf{S}(0)$. This method is much faster because the norm is automatically conserved in the evolution, so the temporal step might be bigger without increasing the error.

We apply these methods to solve the LLG equation in our model for $Mn_3Ir$ along Chapter 2. We consider exchange interaction among nearest neighbours (NN), easy axis anisotropy along $\mathbf{n}_r$ directions, and hard axis anisotropy along $\hat{\mathbf{z}}$ direction, the Hamiltonian which describes this interactions is given by

$$\mathcal{H} = J\sum_{<\mathrm{i},j>}\mathbf{S}_{\mathrm{i}}\cdot\mathbf{S}_j - K\sum_{\mathrm{i}}(\mathbf{S}_{\mathrm{i}}\cdot\mathbf{n}_{\mathrm{i}})^2 + K_z\sum_{\mathrm{i}}(\mathbf{S}_{\mathrm{i}}\cdot\hat{\mathbf{z}}_{\mathrm{i}})^2, \tag{B.7}$$

from where arises an effective field at the position of $\mathbf{S}_{\mathrm{i}}$,

$$\mathbf{B}_{\mathrm{eff}} = J\sum_{j\in\mathrm{NN}(\mathbf{S}_{\mathrm{i}})}\mathbf{S}_j - 2K\sum_{\mathrm{i}}(\mathbf{S}_{\mathrm{i}}\cdot\mathbf{n}_{\mathrm{i}})\mathbf{n}_{\mathrm{i}} + 2K_z\sum_{\mathrm{i}}(\mathbf{S}_{\mathrm{i}}\cdot\hat{\mathbf{z}}_{\mathrm{i}})\hat{\mathbf{z}}_{\mathrm{i}}. \tag{B.8}$$

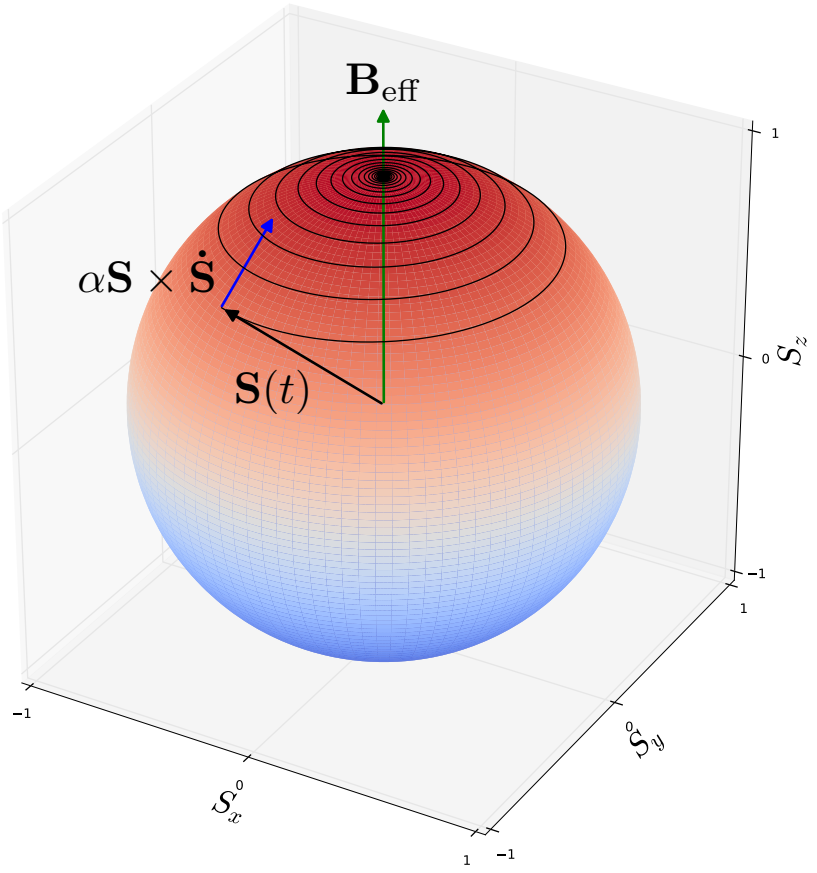


Figure B.1: Time resolved dynamics of a single magnetic moment $\mathbf{S}(t)$ described by the LLG equation. The direction of the magnetic moment is represented by the black arrow. The green arrow correspond to the effective field $\mathbf{B}_{\text{eff}}$ which arises from the contributions to the Hamiltonian. The blue arrow represents the Gilbert damping direction which induces the magnetic moment to align with the effective field. In absence of damping the magnetic moment just precesses around the effective field and never aligns along the effective field.

# Appendix C

# Action of the kagome lattice

Our approach to find an effective theory for the kagome lattice will take the following path [44]. Let's consider a magnetic kagome lattice as in Fig.C.1. The action of the system consists of three terms

$$\mathcal{S} = \sum_k \int \mathrm{d}t\ \hbar \mathbf{A}[\mathbf{S}_k]\cdot\partial_t \mathbf{S}_k - J \sum_{<k,m>} \int \mathrm{d}t\ \mathbf{S}_k\cdot\mathbf{S}_m + K\sum_k \int \mathrm{d}t\ (\mathbf{S}_k\cdot\hat{n}_k)^2 - K_z \sum_k \int \mathrm{d}t\ (\mathbf{S}_k\cdot\hat{z})^2, \tag{C.1}$$

where each in $k$ sum is taken over all sites of the system. The first term is the kinetic term related with the Berry phase, where $\mathbf{A}$ is the vector potential of a magnetic monopole with $4\pi$ flux such that $\int \mathbf{A}(\mathbf{\Omega})\mathrm{d}\mathbf{\Omega}$ is the solid angle reached by $\mathbf{\Omega}$ on the sphere $S_2$ as we have shown in Appendix A. The second term is the Heisenberg interaction among first neighbours in the lattice and the last two terms are an anisotropic interaction defined on each site of the lattice. We choose the antiferromagnetic regime by setting $J > 0$. We also set $K > 0$ to induce the spins to be aligned along the in-plane anisotropy directions, and $K_z < 0$ as a hard anisotropy axis out of plane.

## C.1 A new order parameter

The exchange interaction favors a non-collinear configuration as is possible to deduce from the analysis of an isolated equilateral triangle. All these states are related by a continuous rotation and as this does not change the energy of the system there is an infinite degeneration in energy of the ground state. The anisotropy field on the system breaks the rotational symmetry of the ground states favoring two ordered states, Fig.C.1 shows one of these configurations (the other corresponds to opposite direction of the red arrows). To write the effective Lagrangian of the system we propose to analyze a rotation of the triad of vectors $\hat{n}$ defined before separating the hole system into triangular plaquettes, and study the dynamics of the system in terms of the equations of motion of this rotation $R$. Our approach also consists into add a small unstaggered quantity $\mathbf{L}$ defined on each triangular plaquette. This quantity is analogous to the *canting field* in collinear AF.

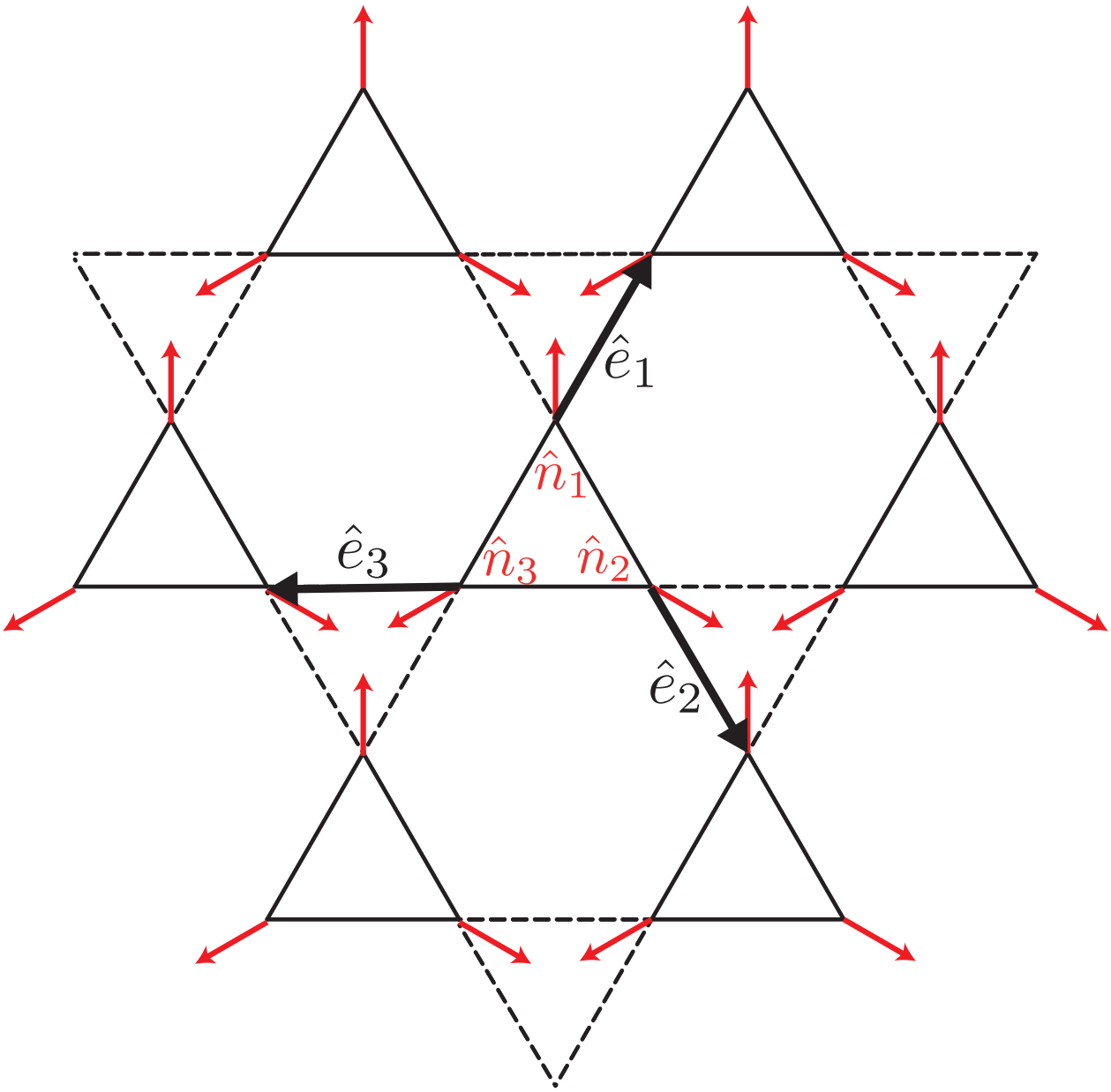


Figure C.1: Cartoon of the vectors utilized in the continuum expansion. In black are the vectors $\hat{e}$, these vectors are used in the expansion of the value of $\mathbf{S}$ in the continuum approximation. $\hat{e}_1 = (\cos\pi/3, \sin\pi/3, 0)$, $\hat{e}_2 = (\cos\pi/3, -\sin\pi/3, 0)$, $\hat{e}_3 = (-1, 0, 0)$. The distance between triangles is $2a$.

We represent each spin in a triangular plaquette as a rotation of the corresponding vector $\hat{n}$ plus the canting field $L$

$$\mathbf{S}_p = \frac{SR(\hat{n}_p + a\mathbf{L})}{\sqrt{1 + 2a\hat{n}_p \cdot L + a^2L^2}}, \tag{C.2}$$

with $p = \{1, 2, 3\}$. In the later sections we will assume $S = 1$. Up to first order in $\mathbf{L}$ in C.2

$$\mathbf{S}_p = R\left(\hat{n}_p + a\left[\mathbf{L} - (\mathbf{L} \cdot \hat{n}_p)\hat{n}_p\right]\right), \tag{C.3}$$

Then, the sum of three spins in a plaquette is

$$\begin{aligned}
\mathbf{S}_1+\mathbf{S}_2+\mathbf{S}_3 &= R[\overbrace{\hat{n}_1+\hat{n}_2+\hat{n}_3}^{=0}-3a\mathbf{L}-a\sum_{\mathrm{i}}(\mathbf{L}_{\mathrm{i}}\cdot\hat{n}_{\mathrm{i}})\hat{n}_{\mathrm{i}}] \\
&= 3aR[\mathbf{L}-\frac{1}{3}\sum_{\mathrm{i}}(\mathbf{L}\cdot\hat{n}_{\mathrm{i}})\hat{n}_{\mathrm{i}}] \\
\Rightarrow \mathbf{S}_1+\mathbf{S}_2+\mathbf{S}_3 &= 3aRT\mathbf{L}. \qquad \text{(C.4)}
\end{aligned}$$

$T$ is a symmetric tensor defined as

$$T_{\mathrm{i}j}=\delta_{\mathrm{i}j}-\frac{1}{3}\sum_k n_{\mathrm{i}}^k n_j^k. \qquad \text{(C.5)}$$

## C.2 Effective action

### C.2.1 Kinetic term

As $\mathbf{S}_p=R\hat{n}_p+aR\boldsymbol{\Delta}_p$, with $\boldsymbol{\Delta}_p=\mathbf{L}-(\mathbf{L}\cdot\hat{n}_p)\hat{n}_p$, then expanding into series the first term in Eq. (C.1) (in this section the square brackets means that the function is evaluated at that argument)

$$A_\alpha[\mathbf{S}](\partial_t\mathbf{S})_\alpha=A_\alpha[R\hat{n}]\partial_t(R\hat{n})_\alpha+\underbrace{A_\alpha[R\hat{n}]\partial_t(aR\Delta)_\alpha+\frac{\partial A_\alpha}{\partial\Omega_k}(aR\Delta)_k\partial_t(R\hat{n})_\alpha}_{\aleph}, \qquad \text{(C.6)}$$

where

$$\begin{aligned}
\frac{\aleph}{a} &= \frac{\partial A_\alpha[R\hat{n}]}{\partial\Omega_k}(R\Delta)_k\partial_t(R\hat{n})_\alpha+A_\alpha[R\hat{n}]\partial_t(R\Delta)_\alpha \\
&= \frac{\partial A_\alpha[R\hat{n}]}{\partial\Omega_k}(R\Delta)_k\partial_t(R\hat{n})_\alpha-\frac{\partial A_k[R\hat{n}]}{\partial\Omega_\alpha}(R\Delta)_k\partial_t(R\hat{n})_\alpha \\
&= \left(\frac{\partial A_\alpha[R\hat{n}]}{\partial\Omega_k}-\frac{\partial A_k[R\hat{n}]}{\partial\Omega_\alpha}\right)(R\Delta)_k\partial_t(R\hat{n})_\alpha, \qquad \text{(C.7)}
\end{aligned}$$

but by the definition of the vector potential

$$\begin{aligned}
\Omega_\alpha &= \varepsilon_{\alpha\beta\gamma}\frac{\partial A_\beta}{\partial\Omega_\gamma}, \\
\Rightarrow \varepsilon_{\alpha\rho\sigma}\Omega_\alpha &= (\delta_{\beta\rho}\delta_{\gamma\sigma}-\delta_{\beta\sigma}\delta_{\gamma\rho})\frac{\partial A_\beta}{\partial\Omega_\gamma}=\frac{\partial A_\rho}{\partial\Omega_\sigma}-\frac{\partial A_\sigma}{\partial\Omega_\rho}. \qquad \text{(C.8)}
\end{aligned}$$

So ℵ becomes

$$\begin{aligned}\frac{\aleph}{a} &= \varepsilon_{\gamma\alpha\beta}\Omega_\gamma(R\Delta)_\beta\partial_t(R\hat{n})_\alpha \\ &= \varepsilon_{\gamma\alpha\beta}(R\hat{n})_\gamma(R\Delta)_\beta\partial_t(R\hat{n})_\alpha \\ &= \varepsilon_{\gamma\alpha\beta}R_{\gamma\mu}\hat{n}_\mu R_{\beta\nu}\Delta_\nu\partial_t(R_{\alpha\varepsilon}\hat{n}_\varepsilon) \\ &= \varepsilon_{\gamma\alpha\beta}R_{\gamma\mu}R_{\beta\nu}\underbrace{\delta_{\alpha\alpha'}}_{R_{\alpha\sigma}R^{-1}_{\sigma\alpha'}}\partial_t(R_{\alpha'\varepsilon}\hat{n}_\varepsilon)\hat{n}_\mu\Delta_\nu \\ &= \varepsilon_{\mu\sigma\nu}(R^{-1}\partial_t R)_{\sigma\varepsilon}\hat{n}_\varepsilon\hat{n}_\mu\Delta_\nu\ . \end{aligned} \tag{C.9}$$

With this previous result we are able to write the first term in Eq. (C.1) as

$$\sum_k \mathbf{A}[\mathbf{S}^k]\cdot\partial_t\mathbf{S}^k = \sum_k \mathbf{A}[R\hat{n}^k]\cdot\partial_t R\hat{n}^k + \underbrace{a\sum_k \varepsilon_{\mu\sigma\nu}(R^{-1}\partial_t R)_{\sigma\varepsilon}\hat{n}^k_\varepsilon\hat{n}^k_\mu\Delta^p_\nu}_{\Lambda}. \tag{C.10}$$

Now we move the sum on the $p$ index (which runs in the sites of one plaquette) to the right of $R$ and assume that $R$ and $\mathbf{L}$ take their values at the same site,

$$\frac{\Lambda}{a} = \varepsilon_{\mu\sigma\nu}(R^{-1}\partial_t R)_{\sigma\varepsilon}\sum_p \Delta^p_\nu\hat{n}^p_\varepsilon\hat{n}^p_\mu. \tag{C.11}$$

As $R\in SO(3)$ the term $(R^{-1}\partial_t R)_{\sigma\varepsilon}$ is antisymmetric. That is demonstrated now:

$$\begin{aligned}(R^{-1}R)_{\alpha\gamma} = R^{-1}_{\alpha\beta}R_{\beta\gamma} &= \delta_{\alpha\gamma} \quad /\partial_t \\ \Rightarrow \partial_t R^{-1}_{\alpha\beta}R_{\beta\gamma} &= -R^{-1}_{\alpha\beta}\partial_t R_{\beta\gamma} \\ R^{-1}_{\gamma\beta}\partial_t R_{\beta\alpha} &= -R^{-1}_{\alpha\beta}\partial_t R_{\beta\gamma} \\ \Rightarrow (R^{-1}\partial_t R)_{\gamma\alpha} &= -(R^{-1}\partial_t R)_{\alpha\gamma}. \end{aligned} \tag{C.12}$$

Due to the antisymmetry of $(R^{-1}\partial_t R)_{\gamma\alpha}$ we can write $(R^{-1}\partial_t R)_{\gamma\alpha} = -\varepsilon_{\lambda\gamma\alpha}V_\lambda$. Using this property, then Equation C.11 can be written as,

$$\begin{aligned}\frac{\Lambda}{a} &= -\varepsilon_{\mu\sigma\nu}\varepsilon_{\lambda\sigma\varepsilon}V_\lambda\sum_p \Delta^p_\nu\hat{n}^p_\varepsilon\hat{n}^p_\mu \\ &= V_\lambda\sum_p \Delta^p_\lambda\underbrace{\hat{n}^p_\mu\hat{n}^p_\mu}_{=1} - V_\lambda\sum_p \Delta^p_\nu\hat{n}^p_\nu\hat{n}^p_\lambda \\ &= V_\lambda\left(\sum_p \Delta^p_\lambda - \sum_p \Delta^p_\nu\hat{n}^p_\nu\hat{n}^p_\lambda\right). \end{aligned} \tag{C.13}$$

If we keep an eye on the last parenthesis

$$\sum_p \Delta^p_\lambda = \sum_p L_\lambda - (\mathbf{L}\cdot\hat{n}^p)\hat{n}^p_\lambda = \sum_\triangle 3(T\mathbf{L})_\lambda, \tag{C.14}$$

and also,

$$\sum_k(\boldsymbol{\Delta}^k\cdot\hat{n}^k)\hat{n}^k_\lambda = \sum_k[\mathbf{L}\cdot\hat{n}^k - (\mathbf{L}\cdot\hat{n}^k)\hat{n}^k_\lambda\hat{n}^k_\lambda] = 0. \tag{C.15}$$

Finally the second term of Equation (C.10) can be written as,

$$\Lambda = \sum_{\triangle} 3aT\mathbf{L}\cdot\mathbf{V}. \tag{C.16}$$

It is important to notice that the sum in $\triangle$ is taken around triplets of spins, as we have utilized the identity given by (C.4); while the sum in $k$ is taken around each site.

With all the calculations made just before we are able to write the kinetic term of the action defined in (C.1) as,

$$\mathcal{K} = \int \mathrm{d}t\ \hbar\left(\sum_{k}\mathbf{A}[R\hat{n}^p]\cdot\partial_t R\hat{n}^p + \sum_{\triangle} 3aT\mathbf{L}\cdot\mathbf{V}\right). \tag{C.17}$$

In a variation of $\mathcal{K}$ just survives his second term because the first term is a topological invariant [44].

### C.2.2 Exchange term

For the calculation of the exchange term we use a Taylor expansion up to second order in derivatives of $\mathbf{S}_{\mathrm{i}}^{\ell+\hat{\mathrm{e}}}$ around $\mathbf{S}_{\mathrm{i}}^{\ell}$, where $\ell$ is the position of spin of species $\mathrm{i}=1,2,3$ in the lattice , then,

$$\mathbf{S}_{\mathrm{i}}^{\ell+\hat{\mathrm{e}}} = \mathbf{S}_{\mathrm{i}}^{\ell} + a(\hat{\mathrm{e}}\cdot\nabla)\mathbf{S}_{\mathrm{i}}^{\ell} + \frac{a^2}{2}(\hat{\mathrm{e}}\cdot\nabla)^2\mathbf{S}_{\mathrm{i}}^{\ell}, \tag{C.18}$$

where $a$ is the lattice constant. The vectors $\hat{\mathrm{e}}_{\mathrm{i}}$ are shown in Fig. C.1, and they allow us to write the interaction among first neighbours of the whole system in terms of only three products. The interaction energy depends on the different position $\ell$ of the spins in the different plaquettes $\triangle$, so,

$$\mathcal{H} = J\sum_{\triangle}\mathbf{S}_1^{\ell}\cdot(\mathbf{S}_3^{\ell-\hat{\mathrm{e}}_1}+\mathbf{S}_3^{\ell+\hat{\mathrm{e}}_1}) + \mathbf{S}_2^{\ell}\cdot(\mathbf{S}_1^{\ell-\hat{\mathrm{e}}_2}+\mathbf{S}_1^{\ell+\hat{\mathrm{e}}_2}) + \mathbf{S}_3^{\ell}\cdot(\mathbf{S}_2^{\ell-\hat{\mathrm{e}}_3}+\mathbf{S}_2^{\ell+\hat{\mathrm{e}}_3}). \tag{C.19}$$

Expanding as in Eq.C.18 we get (we omit the superscript $\ell$ because is the same for each term in the expression),

$$\begin{aligned}\mathcal{H} = J\sum_{\triangle} & 2(\mathbf{S}_1\cdot\mathbf{S}_3+\mathbf{S}_2\cdot\mathbf{S}_1+\mathbf{S}_3\cdot\mathbf{S}_2) \\ & + \underbrace{a^2[\mathbf{S}_1\cdot(\hat{\mathrm{e}}_1\cdot\nabla)^2\mathbf{S}_3+\mathbf{S}_2\cdot(\hat{\mathrm{e}}_2\cdot\nabla)^2\mathbf{S}_1+\mathbf{S}_3\cdot(\hat{\mathrm{e}}_3\cdot\nabla)^2\mathbf{S}_2]}_{\Upsilon},\end{aligned} \tag{C.20}$$

The first term is just $(\mathbf{S}_1+\mathbf{S}_2+\mathbf{S}_3)^2$ plus a constant as we have shown before, and by the result of Sec.C.1 this term is just $9a^2(T\mathbf{L})^2$. Recalling that $\mathbf{S}_p = R\hat{n}_p + aR\boldsymbol{\Delta}_p$, we get,

$$\Upsilon = a^2R^{\alpha\beta}\partial_{\mathrm{i}}\partial_j R^{\alpha\gamma}\Gamma^{\mathrm{i}j}_{\beta\gamma} + \mathcal{O}(a^3), \tag{C.21}$$

where the tensor $\Gamma$ is defined as,

$$\Gamma^{\mathrm{i}j}_{\beta\gamma} = \hat{\mathrm{e}}_1^{\mathrm{i}}\hat{\mathrm{e}}_1^{j}n_1^{\beta}n_3^{\gamma} + \hat{\mathrm{e}}_2^{\mathrm{i}}\hat{\mathrm{e}}_2^{j}n_2^{\beta}n_1^{\gamma} + \hat{\mathrm{e}}_3^{\mathrm{i}}\hat{\mathrm{e}}_3^{j}n_3^{\beta}n_2^{\gamma}. \tag{C.22}$$

As $\partial_{\rm i}(R^{-1}\partial_j R)^{\alpha\gamma} = (R^{-1}\partial_{\rm i}\partial_j R)^{\alpha\gamma} - [(R^{-1}\partial_{\rm i}R)(R^{-1}\partial_j R)]^{\alpha\gamma}$, then the exchange interaction is reduced (up of a total derivative) to,

$$\mathcal{H} = J\sum_{\triangle} 9a^2(T\mathbf{L})^2 + a^2[(R^{-1}\partial_{\rm i}R)(R^{-1}\partial_j R)]^{\beta\gamma}\Gamma^{{\rm i}j}_{\beta\gamma}. \tag{C.23}$$

### C.2.3 Anisotropy term

We can write the anisotropy term depending of $\hat{n}$ instead of $\hat{\rho}$ because they are anti-parallel. So we have,

$$\mathcal{A} = K\sum_{\triangle}(\mathbf{S}_1\cdot\hat{n}_1)^2 + (\mathbf{S}_2\cdot\hat{n}_2)^2 + (\mathbf{S}_3\cdot\hat{n}_3)^2, \tag{C.24}$$

then,

$$\Rightarrow \mathcal{A} = K\sum_{\triangle}\sum_{p}^{3}(\hat{n}_p\cdot R\hat{n}_p)^2 + 2a(\hat{n}_p\cdot R\hat{n}_p)(\hat{n}_p\cdot R\boldsymbol{\Delta}_p) + a^2(\hat{n}_p\cdot\mathbf{L})(\hat{n}_p\cdot R\mathbf{L}). \tag{C.25}$$

Nevertheless, we have considered that the field $R$ changes smoothly along the lattice, so the projection of each rotated $\hat{n}$ on the original is nearly the same for each site in a plaquette. Then it is possible to approximate the easy axis anisotropy term as just the first term of Eq. C.25,

$$\begin{aligned}\mathcal{A} =& K\sum_{\triangle}\sum_{p}^{3}(\hat{n}_p\cdot R\hat{n}_p)^2 + a^2(\hat{n}_p\cdot R\hat{n}_p)^2L^2 + a^2\left[(\hat{n}_p\cdot R\mathbf{L})^2 - 2(\hat{n}_p\cdot\mathbf{L})(\hat{n}_p\cdot R\mathbf{L})\right]\\ \approx& K\sum_{\triangle}\sum_{p}^{3}(\hat{n}_p\cdot R\hat{n}_p)^2.\end{aligned} \tag{C.26}$$

The hard anisotropy axis in $\hat{\mathbf{z}}$ is simply

$$\mathcal{A}_z = -K_z\sum_{\triangle}\sum_{p}^{3}(\hat{\mathbf{z}}\cdot R\hat{n}_p)^2. \tag{C.27}$$

### C.2.4 The Lagrangian

With the previous sections, we are now in conditions to write the action of the system in terms of the new parameter $R$ and his derivatives,

$$\begin{aligned}\mathcal{S} = \int \mathrm{d}t\sum_k \hbar\mathbf{A}[R\hat{n}^k]\cdot\partial_t R\hat{n}^k + \sum_{\triangle} 3\hbar a(T\mathbf{L})\cdot\mathbf{V} - 9Ja^2(T\mathbf{L})^2\\ - Ja^2[(R^{-1}\partial_{\rm i}R)(R^{-1}\partial_j R)]^{\beta\gamma}\,\Gamma^{{\rm i}j}_{\beta\gamma} + K\sum_{p}^{3}(\hat{n}_p\cdot R\hat{n}_p)^2 - K_z\sum_{p}^{3}(\hat{\mathbf{z}}\cdot R\hat{n}_p)^2.\end{aligned} \tag{C.28}$$

As the first term disappears in the variation of $\mathcal{S}$, we write the Lagrangian density as,

$$\mathcal{L} = \sum_{\triangle} 3\hbar a(T\mathbf{L})\cdot\mathbf{V} - 9Ja^2(T\mathbf{L})^2 - Ja^2[(R^{-1}\partial_{\mathrm{i}}R)(R^{-1}\partial_j R)]^{\beta\gamma}\ \Gamma^{\mathrm{i}j}_{\beta\gamma} + K\sum_p^3(\hat{n}_p\cdot R\hat{n}_p)^2 - K_z\sum_p^3(\mathbf{z}\cdot R\hat{n}_p)^2. \quad \text{(C.29)}$$

### C.2.5 Effective action and non-linear $\sigma$ model

In the long wavelength limit approximate our discrete system by a continuous one. This means that we make the following replacement

$$\sum_{\triangle} \to \int \mathrm{d}x\ \mathrm{d}y \frac{4}{\sqrt{3}a^2}, \quad \text{(C.30)}$$

where the numerical factor is nothing but the area of a triangle with side $2a$. In this limit the effective Lagrangian density for the system becomes,

$$\mathcal{L} = \frac{4\sqrt{3}}{a}\hbar T\mathbf{L}\cdot\mathbf{V} - 12\sqrt{3}J(T\mathbf{L})^2 - \frac{4J}{\sqrt{3}}[(R^{-1}\partial_{\mathrm{i}}R)(R^{-1}\partial_j R)]^{\beta\gamma}\ \Gamma^{\mathrm{i}j}_{\beta\gamma} + \frac{4K}{\sqrt{3}a^2}\sum_{\mathrm{i}}^3(\hat{n}_{\mathrm{i}}\cdot R\hat{n}_{\mathrm{i}})^2 - \frac{4K_z}{\sqrt{3}a^2}\sum_{\mathrm{i}}^3(\hat{\mathbf{z}}\cdot R\hat{n}_{\mathrm{i}})^2. \quad \text{(C.31)}$$

Now we proceed to solve the Euler-Lagrange equations for the field $T\mathbf{L}$ to get a Lagrangian density only depending on the field $R$. As the action is quadratic in $T\mathbf{L}$, this is analogous to perform a Gaussian integral in the action to integrate the high energy modes in the action. We proceed then calculating the equation of motion of the field $T\mathbf{L}$,

$$\frac{\partial\mathcal{L}}{\partial(T\mathbf{L})} = \frac{4\sqrt{3}\hbar}{a}\mathbf{V} - 24\sqrt{3}J(T\mathbf{L}) = 0$$
$$\Rightarrow T\mathbf{L} = \frac{\hbar\mathbf{V}}{6Ja}. \quad \text{(C.32)}$$

We utilize this result in equation (C.31) to get

$$\mathcal{L} = \frac{\hbar^2}{\sqrt{3}Ja^2}\mathbf{V}\cdot\mathbf{V} - \frac{4J}{\sqrt{3}}[(R^{-1}\partial_{\mathrm{i}}R)(R^{-1}\partial_j R)]^{\beta\gamma}\Gamma^{\mathrm{i}j}_{\beta\gamma} + \frac{4K}{\sqrt{3}a^2}\sum_{\mathrm{i}}(\hat{n}_{\mathrm{i}}\cdot R\hat{n}_{\mathrm{i}})^2 - \frac{4K_z}{\sqrt{3}a^2}\sum_{\mathrm{i}}(\hat{\mathbf{z}}\cdot R\hat{n}_{\mathrm{i}})^2. \quad \text{(C.33)}$$

Recalling that $V_\lambda = -\frac{1}{2}\varepsilon_{\lambda\mu\nu}(R^{-1}\partial_t R)_{\mu\nu}$, then $\mathbf{V}\cdot\mathbf{V} = -\frac{1}{2}\mathrm{Tr}[(R^{-1}\partial_t R)^2]$, so the Lagrangian can be finally written as,

$$\mathcal{L} = -\frac{\hbar^2}{2\sqrt{3}Ja^2}\mathrm{Tr}[(R^{-1}\partial_t R)^2] - \frac{4J}{\sqrt{3}}[(R^{-1}\partial_{\mathrm{i}}R)(R^{-1}\partial_j R)]^{\beta\gamma}\Gamma^{\mathrm{i}j}_{\beta\gamma} + \frac{4K}{\sqrt{3}a^2}\sum_{\mathrm{i}}(\hat{n}_{\mathrm{i}}\cdot R\hat{n}_{\mathrm{i}})^2 - \frac{4K_z}{\sqrt{3}a^2}\sum_{\mathrm{i}}(\hat{\mathbf{z}}\cdot R\hat{n}_{\mathrm{i}})^2. \quad \text{(C.34)}$$

This last equation is also known as the non-linear $\sigma$ model of SO(3).

## C.3 Spin wave spectra

In this section we briefly show the calculation of the spin wave spectra starting from our effective theory for $Mn_3Ir$. For this we parameterize the small deviations from equilibrium by making use of Euler's rotation matrix $R(\phi,\theta,\psi) = R_Z(\psi)R_X(\theta)R_z(\phi)$. The resulting Lagrangian is awful and is too difficult to write it down here, but it is possible to calculate first order perturbations around these angles.

### C.3.1 Euler angles

We name Euler's angles by the triplet $(\phi,\theta,\psi)$. Figure C.2 shows the definition of each angle. Then the rotation matrix

$$\begin{aligned} R(\phi,\theta,\psi) &= R_Z(\psi)R_X(\theta)R_z(\phi) \\ &= \begin{pmatrix} \cos\psi\cos\phi - \cos\theta\sin\psi\sin\phi & -\cos\theta\sin\psi\cos\phi - \cos\psi\sin\phi & \sin\theta\sin\psi \\ \cos\theta\cos\psi\sin\phi + \sin\psi\cos\phi & \cos\theta\cos\psi\cos\phi - \sin\psi\sin\phi & -\sin\theta\cos\psi \\ \sin\theta\sin\phi & \sin\theta\cos\phi & \cos\theta \end{pmatrix}. \end{aligned} \tag{C.35}$$

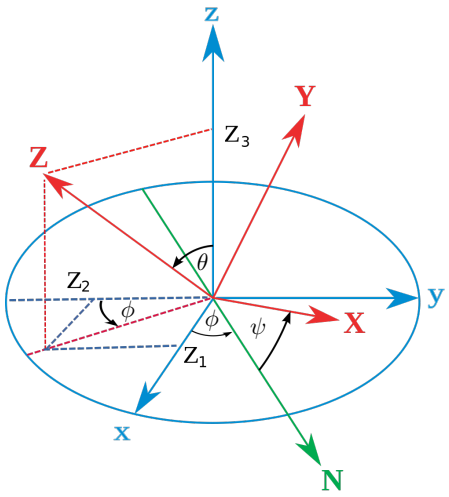


Figure C.2: Cartoon of the definition of Euler angles. This angles are used in the calculation of the spin wave spectra of the system.

### C.3.2 Perturbation of homogeneous state

Now we calculate perturbations around the homogeneous state

$$(\phi,\theta,\psi) = (0+\delta\phi, 0+\delta\theta, 0+\delta\psi),$$

obtaining the following Lagrangian up to second order in $\delta$ (here $\delta\chi = \delta\phi + \delta\psi$),

$$\mathcal{L}_{2\text{nd}} = \frac{\hbar^2}{\sqrt{3}a^2 J}\left[\dot{\delta\theta}^2 + \dot{\delta\chi}^2\right] - \frac{2\sqrt{3}}{a^2}(K + K_z)\delta\theta^2 - \frac{4\sqrt{3}K}{a^2}\delta\chi^2 - 3J\delta\chi'^2 \quad \text{(C.36)}$$

The equations of motion of this Lagrangian are,

$$\ddot{\delta\chi} + \frac{3Ja^2}{\hbar^2}\delta\chi'' - \frac{12JK}{\hbar^2}\delta\chi = 0, \quad \text{(C.37)}$$

$$\ddot{\delta\theta} + \frac{6J(K + K_z)}{\hbar^2}\delta\theta = 0. \quad \text{(C.38)}$$

From here it is straightforward to obtain the spin wave spectra shown in Sec. 2.3

# Appendix D

# Sine-Gordon solitons

Solitons are a particular solution of the SGE and are present in a lot of different contexts, as Josephson junctions, coupled pendula, dislocations, and a wide list of physical phenomena [50]. Here we show how they arise from the effective theory for the magnetization field of a non collinear antiferromagnet.

## D.1 Sine-Gordon equation from effective theory

In Appendix C we have shown explicitly that the effective Lagrangian of an antiferromagnetic spin system with the named anisotropies in a kagome lattice is given by Eq.C.34. If we make the assumption that $R$ is a rotation around $\hat{z}$ direction (perpendicular to the plane) defined at each point of the space by the angle $\phi(x)$, i .e

$$R = R(\phi, \hat{z}) = \begin{pmatrix} \cos\phi & -\sin\phi & 0 \\ \sin\phi & \cos\phi & 0 \\ 0 & 0 & 1 \end{pmatrix},$$

the Lagrangian of Eq.C.34 becomes,

$$\mathcal{L} = \frac{\hbar^2}{\sqrt{3}a^2 J}(\partial_t\phi)^2 - \sqrt{3}J[(\partial_x\phi)^2 + (\partial_y\phi)^2] + \frac{4\sqrt{3}K}{a^2}\cos^2\phi. \tag{D.1}$$

The equations of motion for $\phi$ are computed using the Euler-Lagrange equation,

$$\partial_{tt}\phi - \frac{3J^2a^2}{\hbar^2}\nabla^2\phi + \frac{6JK}{\hbar^2}\sin(2\phi) = 0. \tag{D.2}$$

The last equation is nothing but a sine-Gordon equation for the field $\phi$, which in a general form is written as

$$\partial_{tt}\phi - c^2\nabla^2\phi + \frac{m^2c^4}{\hbar^2}\sin(2\phi) = 0, \tag{D.3}$$

so there is possible to identify the speed $c^2 = 3J^2a^2/\hbar^2$ and the mass term $m^2c^4/\hbar^2 = 6JK/\hbar^2$.

## D.2 Solutions of sine-Gordon equation and Bäcklund transformations

The sine-Gordon equation might be written as

$$\partial_{tt}\varphi - \nabla^2\varphi + \sin\varphi = 0. \tag{D.4}$$

This equation is related with the 'physical' equation by the transformation

$$t \to \frac{\hbar}{\sqrt{2}mc^2}t; \;\; x \to \frac{\hbar}{\sqrt{2}mc}x; \;\; \varphi \to 2\phi. \tag{D.5}$$

In order to find a solution of this equation we can do an straightforward integration . Also there is possible to use a more elegant method called Bäcklund transformations which allows to find additional solutions of a partial differential equation (PDE) if one particular solution is known. Here we show both roads, beginning by a brute force integration.

### D.2.1 Brute force solution

If we set $u = x - vt$, then $\partial_{tt}\varphi(x,t) = v^2\varphi(u)''$ and $\nabla^2\varphi(x,t) = \varphi(u)''$, so Eq. (D.4) becomes

$$\varphi'' = \frac{\sin\varphi}{1-v^2}. \tag{D.6}$$

We notice that there is a conserved quantity. This can be seen by multiplying Eq.(D.6) by $2\varphi'$, then

$$2\varphi'\left(\varphi'' - \frac{\sin\varphi}{1-v^2}\right) = \frac{\partial}{\partial u}\left(\varphi'^2 + \frac{2\cos\varphi}{1-v^2}\right) = 0 \Rightarrow \varphi'^2 + \frac{2\cos\varphi}{1-v^2} = K = \text{constant}. \tag{D.7}$$

This constant is fixed by boundary conditions. If we set $\varphi'(u \to \pm\infty) = 0$, $\varphi(u \to -\infty) = 0$ and $\varphi(u \to \infty) = 2\pi$, then

$$K = \frac{2}{1-v^2}.$$

So the Eq.(D.7) might be written as

$$\varphi'^2 = \frac{2}{1-v^2}(1-\cos\varphi).$$

By elementary trigonometry identities as $\cos x/2 = \cos^2 x/4 - \sin^2 x/4$,

$$\varphi'^2 = \frac{2}{1-v^2}\sin^2\frac{\varphi}{2}.$$

Integrating we get

$$\int_{u_0}^{u} \mathrm{d}u = \pm\frac{\sqrt{1-v^2}}{2}\int_{\varphi(u_0)}^{\varphi(u)} \frac{\mathrm{d}\varphi}{\sin(\varphi/2)}. \tag{D.8}$$

Without losing generality we set $u_0 = 0$, then

$$\int_{\pi/2}^{\varphi(u)} \frac{\mathrm{d}\varphi}{\sin(\varphi/2)} = \log\left|\frac{\cos(\varphi(u)/2)-1}{\cos(\varphi(u)/2)+1}\right| + C$$

$$\Rightarrow \frac{u}{\sqrt{1-v^2}} = \pm\frac{1}{2}\log\left|\frac{\cos(\varphi(u)/2)-1}{\cos(\varphi(u)/2)+1}\right| + C = \pm\log|\tan(\varphi/4)| + C.$$

Is straight forward to find the solution for $\varphi$, as $u = x - vt$,

$$\varphi(x,t) = 4\arctan\left[C\exp\left(\frac{x-vt}{\sqrt{1-v^2}}\right)\right], \tag{D.9}$$

$C$ is an integration constant fixed by the boundary conditions. This solution is known as the *kink* solution.

## D.3 Bäcklund transformation

Another way to find a family of solutions it is standard to use the method called Bäcklund transformations. The main idea behind this method is that if we know a solution of a PDE, even if is trivial, then exist a transformation which transforms one solution into another solution. To be more specific consider that we want to solve the PDE $E(\phi) = 0$ where $E$ is a differential operator. Now consider another PDE $D(\varphi) = 0$. Then is possible to find two relations between $\phi$ and $\varphi$ which we call $R_\mathrm{i}$,

$$R_1(\phi, \varphi, \ldots; x, t) = 0,$$

$$R_2(\phi, \varphi, \ldots; x, t) = 0.$$

We say that $R_\mathrm{i}$ is a Bäcklund transformation if:

(1) The relations $R_\mathrm{i}$ are integrable for $\varphi$ when $E(\phi) = 0$.
(2) The resulting $\varphi$ must be a solution of $D(\varphi)$.
(3) Vice-versa also must be true.

In order to clarify this method we show an example which is of interest for the development of this work.

### D.3.1 Bäcklund transformation for SG-E

The Bäcklund transformations for the sine-Gordon equation are shown here as an example of the method showed before. First we define the variables $\rho = x + t$ and $\tau = x - t$. This coordinates are called 'light cone' coordinates. Then the D'alembertian operator in this coordinates might be written as

$$(\partial_{tt} - \nabla^2) = (\partial_t + \partial_x)(\partial_t - \partial_x) = \partial_\rho \partial_\tau,$$

so the sine-Gordon equation is reduced to

$$\partial_\rho \partial_\tau \phi = \sin\phi. \tag{D.10}$$

We propose the following transformations (which correspond to the $R_{\rm i}$ relations named before) for two fields $\phi$ and $\varphi$ following the sine-Gordon equation,

$$\partial_\rho \frac{(\phi+\varphi)}{2} = a \sin\left(\frac{\phi-\varphi}{2}\right), \tag{D.11}$$

$$\partial_\tau \frac{(\phi-\varphi)}{2} = \frac{1}{a} \sin\left(\frac{\phi+\varphi}{2}\right), \tag{D.12}$$

To show that those relations lead to the sine-Gordon equation, let's differentiate in $\tau$ the Eq.(D.11), and in $\rho$ the Eq.(D.12)

$$\partial_\tau \partial_\rho \left(\frac{1}{2}(\phi+\varphi)\right) = a\frac{1}{2}\partial_\tau(\phi-\varphi)\cos\left(\frac{\phi-\varphi}{2}\right) = \sin\left(\frac{\phi+\varphi}{2}\right)\cos\left(\frac{\phi-\varphi}{2}\right),$$

$$\partial_\rho \partial_\tau \left(\frac{1}{2}(\phi-\varphi)\right) = \frac{1}{a}\partial_\rho \frac{(\phi+\varphi)}{2}\cos\left(\frac{\phi+\varphi}{2}\right) = \cos\left(\frac{\phi+\varphi}{2}\right)\sin\left(\frac{\phi-\varphi}{2}\right),$$

where the last equality in each equation is achieved by using Eqs.(D.11) and (D.12). Then by adding and subtracting these last equation we find that

$$\partial_\rho \partial_\tau \phi = \sin\phi; \quad \partial_\rho \partial_\tau \varphi = \sin\varphi.$$

So in summary what we have done is basically take a solution $\varphi$ of the sine-Gordon equation, generate another function $\phi$ which fulfills (D.11) and (D.12), and show that this new function $\phi$ is also a solution of sine-Gordon equation. It is impressive but it works.

With all those results in the pocket, let's consider a function $\varphi = 0$, which of course is a solution of sine-Gordon equation. Then by (D.11) and (D.12)

$$\partial_\rho \phi = 2a \sin\left(\frac{\phi}{2}\right); \quad \partial_\tau \phi = \frac{2}{a}\sin\left(\frac{\phi}{2}\right).$$

A straightforward integration lead us to the kink solution

$$\varphi(x,t) = 4\arctan\left[C\exp\left(\frac{x-vt}{\sqrt{1-v^2}}\right)\right], \tag{D.13}$$

where we have identified the velocity of the soliton as $v = (1-a^2)/(1+a^2)$. It can be shown that starting from the kink solution it is possible to find the breather solution.

# Appendix E

# Spin waves of magnonic crystal

In this appendix we show how to solve numerically the spin wave spectra of the antiferromagnetic magnonic crystal of Chapter 3.

## E.1 Spin wave spectra from equations of motion

We start from Eqs. (3.4) and (3.5). By setting

$$\mathbf{n}_0 = \hat{z};$$

$$\delta\mathbf{n} = \{\delta n_x(x)\cos(\omega t), \delta n_y(x)\sin(\omega t), 0\};$$
$$\mathbf{m} = \{m_x(x)\cos(\omega t), m_y(x)\sin(\omega t), 0\},$$

we find that the equations of motion for $\delta\mathbf{n}$ and $\mathbf{m}$ are

$$\delta n_x \frac{\omega}{\gamma} = a m_y + H\delta n_y; \tag{E.1}$$
$$\delta n_y \frac{\omega}{\gamma} = a m_x + H\delta n_x; \tag{E.2}$$
$$m_x \frac{\omega}{\gamma} = -A\nabla^2\delta n_y - K_z\delta n_y + H m_y; \tag{E.3}$$
$$m_y \frac{\omega}{\gamma} = -A\nabla^2\delta n_x + K_z\delta n_x + H m_x. \tag{E.4}$$

This system of equations can be written as

$$\frac{\omega}{\gamma}\begin{pmatrix} \delta n_x \\ \delta n_y \\ m_x \\ m_y \end{pmatrix} = \begin{pmatrix} 0 & H & 0 & a \\ H & 0 & a & 0 \\ 0 & -K_z - A\nabla^2 & 0 & H \\ K_z - A\nabla^2 & 0 & H & 0 \end{pmatrix}\begin{pmatrix} \delta n_x \\ \delta n_y \\ m_x \\ m_y \end{pmatrix}, \tag{E.5}$$

which is just an eigenvalue problem for the above matrix. This problem is solved my making use of LAPACK routines in `C++`.